Biosensors and Bioelectronics 278 (2025) 117321

Contents lists available at ScienceDirect

Biosensors and Bioelectronics

journal homepage: www.elsevier.com/locate/bios

Multimodal fusion of magnetoencephalography and photoacoustic imaging based on optical pump: Trends for wearable and noninvasive Brain–Computer interface

Chengpeng Chai [a,b,1], Xi Yang [a,b,1], Yuqiao Zheng [a,b], Md Belal Bin Heyat [a,b], Yifan Li [c], Dingbo Yang [d,e], Yun-Hsuan Chen [a,b,*], Mohamad Sawan [a,b,**]

[a] CenBRAIN Neurotech, School of Engineering, Westlake University, 600 Dunyu Road, Xihu District, Hangzhou, Zhejiang, 310030, China
[b] Institute of Advanced Technology, Westlake Institute for Advanced Study, 18 Shilongshan Street, Xihu District, Hangzhou, Zhejiang, 310024, China
[c] Faculty of Engineering, University of Bristol, Bristol, BS8 1QU, United Kingdom
[d] Department of Neurosurgery, Affiliated Hangzhou First People's Hospital, Westlake University School of Medicine, Hangzhou, 310000, China
[e] Department of Neurosurgery, Nanjing Medical University Affiliated Hangzhou Hospital, Hangzhou First People's Hospital, Hangzhou, 310000, China

ARTICLE INFO

Keywords:
Brain-computer interfaces
Optical pumped magnetometers-magnetoencephalography
Photoacoustic imaging
Electroencephalography
Functional near-infrared spectroscopy
Multimodal fusion

ABSTRACT

Wearable noninvasive brain–computer interface (BCI) technologies, such as electroencephalography (EEG) and functional near-infrared spectroscopy (fNIRS), have experienced significant progress since their inception. However, these technologies have not achieved revolutionary advancements, largely because of their inherently low signal-to-noise ratio and limited penetration depth. In recent years, the application of quantum-theory-based optically pumped (OP) technologies, particularly optical pumped magnetometers (OPMs) for magnetoencephalography (MEG) and photoacoustic imaging (PAI) utilizing OP pulsed laser sources, has opened new avenues for development in noninvasive BCIs. These advanced technologies have garnered considerable attention owing to their high sensitivity in tracking neural activity and detecting blood oxygen saturation. This paper represents the first attempt to discuss and compare technologies grounded in OP theory by examining the technical advantages of OPM-MEG and PAI over traditional EEG and fNIRS. Furthermore, the paper investigates the theoretical and structural feasibility of hardware reuse in OPM-MEG and PAI applications.

1. Introduction

Morphologically, the brain constitutes a vital element of the central nervous system, specialized in the collection, distribution, storage, and processing of information, rendering it the most complex signal-processing organ (Udovičić et al., 2016). Advancements in neuroscience research have driven the development of brain–computer interfaces (BCIs). These systems differ from technologies that rely solely on accelerometers to detect mobility and posture (Chen and David R Bassett, 2005) or electrocardiograms to monitor cardiovascular conditions (Liu et al., 2021a). A BCI is a system that measures central nervous system (CNS) activity and converts it into artificial outputs to replace, restore, enhance, supplement, or improve natural CNS outputs, altering the ongoing interaction between the CNS and its external or internal environment (Wolpaw et al., 2020). Research on replacement, restoration, and improvement includes not only curing diseases but also adjusting physiological or psychological states, with numerous studies in recent years on disease-related treatments like transcranial electrical stimulation (TES) for epilepsy (Kozák and Berényi, 2017), transcranial magnetic stimulation (TMS) for stroke (Smith and Stinear, 2016), and even meta-analyses (Bai et al., 2020; Cervera et al., 2018), as well as studies on alleviating phantom limb pain (Yanagisawa et al., 2020), depression (Gall et al., 2024), and fatigue wakefulness (Talukdar et al., 2020). Moreover, research involving enhancement and improvement has primarily focused on driving external devices using BCI systems to operate robotic arms (Bousseta et al., 2018; Saragih et al., 2022),

* Corresponding author. CenBRAIN Neurotech, School of Engineering, Westlake University, 600 Dunyu Road, Xihu District, Hangzhou, Zhejiang, 310030, China.
** Corresponding author. Institute of Advanced Technology, Westlake Institute for Advanced Study, 18 Shilongshan Street, Xihu District, Hangzhou, Zhejiang, 310024, China.
E-mail addresses: chenyunxuan@westlake.edu.cn (Y.-H. Chen), sawan@westlake.edu.cn (M. Sawan).
[1] These authors contributed equally to this work.

https://doi.org/10.1016/j.bios.2025.117321
Received 24 October 2024; Received in revised form 19 February 2025; Accepted 26 February 2025
Available online 26 February 2025
0956-5663/© 2025 The Authors. Published by Elsevier B.V. This is an open access article under the CC BY license (http://creativecommons.org/licenses/by/4.0/).

exoskeletons (Choi et al., 2020), humanoid robots (Chae et al., 2012), or drones (Wang et al., 2018), performing tasks deemed dangerous or impractical for humans, such as mine removal (Barngrover et al., 2015).

Such advancements underline the growing demand for noninvasive BCI sensors that not only contribute to a deeper understanding of the brain's complex mechanisms but also play a pivotal role in clinical medicine, neural rehabilitation, and the broader field of human-computer interaction. Noninvasive BCIs can be divided into two categories based on the biological signal type they detect: Electrophysiological-Signal-Activity-Dependent (ESAD) sensors and Blood-Oxygen-Level-Dependent (BOLD) sensors.

ESAD sensors such as electroencephalography (EEG) and magnetoencephalography (MEG) primarily capture the flow of electrons or magnetic fields generated by cellular-level biochemical processes (da Silva, 2013), achieving high temporal resolution at the expense of low spatial resolution (Teplan, 2002). They are suitable for rapid and transient superficial brain activity recording. On the other hand, BOLD sensors such as functional near-infrared spectroscopy (fNIRS) and photoacoustic imaging (PAI) infer brain activity by monitoring changes in brain oxygen levels (Turner and Jones, 2003), offering high spatial resolution but with significant sensing delays (Ferrari and Quaresima, 2012), rendering them suitable for relatively longer-term anomaly monitoring.

Emerging sensors—optical pumped magnetoencephalography (OPM-MEG) and PAI—have garnered significant attention. OPM-MEG is considered to have the potential to surpass EEG and traditional MEG theory, e.g., Superconducting Quantum Interference Devices (SQUIDs), by providing superior data quality, enhanced coverage uniformity, improved robustness against motion, and reduced system complexity (Brookes et al., 2022). Meanwhile, PAI holds the promise of exceeding fNIRS by offering detailed blood oxygen distribution data and enabling deeper, three-dimensional (3D) tissue imaging (Yang et al., 2024b).

The most compelling aspect is that EEG is constrained by the need for electrodes to make direct contact with the skin, imposing a minimum size limit. In contrast, the atomic vapor cells used in MEG, which are designed with technologies such as MEMS, can be as small as 1 mm^3 (Griffith et al., 2010)—far smaller than EEG electrodes. Similarly, fNIRS is limited by the need for multiple independent light sources (Zhou et al., 2020), which cannot be triggered simultaneously, leading to a minimum system size. However, PAI can operate with a single shared light source, and the size constraints of ultrasound transducers are significantly smaller than those of light sources. These factors contribute to the superior wearability potential of OPM-MEG and PAI compared to EEG and fNIRS.

In pursuit of higher temporal and spatial resolution, researchers of noninvasive BCIs have opted for multimodal sensor fusion, integrating ESAD sensors with BOLD sensors (Ahn and Jun 2017). However, this approach also introduces new challenges such as sensor volume, measurement synchronicity, same-site measurement, and interference between multimodal sensors (Ahn and Jun 2017; Everdell et al., 2005; Kassab et al., 2015; Ru et al., 2022; Uchitel et al., 2021; von Lühmann and Müller, 2017; von Lühmann et al., 2016). Notably, due to their close principles in sensing, OPM-MEG and PAI sensors, based on optically pumped sources, show good hardware compatibility, potentially solving issues related to measurement volume, synchronicity, and interference. This review aims to theoretically explore the limitations of these approaches and analyze the feasibility of integrating OPM-MEG and PAI as a solution for improving multimodal BCI systems.

1.1. Contribution of this paper

The literature contains numerous excellent research papers and reviews that provide a variety of perspectives on noninvasive BCIs. The following sections detail and compare these perspectives. In this work, the definitions of wearable and noninvasive BCI devices are clarified, addressing a critical gap in both theoretical research and practical engineering applications. A new architecture for sensor reuses across different dimensions of BCIs is also proposed. The key contributions of this study are presented below.

1. **Identification and update definitions within the BCI domain:** This paper clarifies and updates the definitions of noninvasive/invasive and wearable BCIs based on recent breakthroughs, the applicable range of BCI sensors has been specified, distinctly contrasting with previous studies that considered wearable sensors and BCIs as separate entities.
2. **Discuss advantages and disadvantages of novel noninvasive BCI sensors:** This paper reviews the technological advantages of emerging OPM-MEG and PAI over traditional EEG and fNIRS, emphasizing their potential for more precise and robust data acquisition in BCIs. It also analyzes the design improvements needed for OPM-MEG, such as balancing sensitivity, response nonlinearity, response bandwidth, and minimizing sensor crosstalk. For PAI, it explores solutions for issues like impedance matching, miniaturization of auto-focus light sources, and improving imaging timeliness.
3. **Address multimodal fusion challenges:** This paper identifies the limitations of traditional multimodal measurement techniques and proposes solutions that enable hardware-level reuse between OPM-MEG and PAI. This structure facilitates synchronized measurements at the same location and time, supporting real-time brain monitoring with smaller sensor volumes.

This comprehensive review critically examines the current literature on noninvasive wearable BCIs. To guide further research in this field, unresolved challenges in multimodal approaches are identified, and future research directions are recommended.

1.2. Related work

To the best of our knowledge, this paper is the first to present a comprehensive overview of scientific breakthroughs in noninvasive wearable BCI sensors. It optimizes the existing BCI definitions based on recent breakthroughs and compares the performance and wearable properties of both new and traditional sensors across two major categories: nerve-based and blood-oxygen-based. Finally, future research directions are proposed. Table 1 highlights the key differences in related works published since 2015, with definitions based on the refined version in Section 2.

Existing literature on multimodal noninvasive BCIs primarily focuses on established technologies such as EEG (Uchitel et al., 2021) and fNIRS (Liu et al., 2021b) or newer BCI devices such as PAI (Yang et al., 2021a, b) and OPM-MEG (Aslam et al., 2023), while this review uniquely addresses the integration and advantages of emerging OP technologies—OPM-MEG and PAI—which have not been comprehensively compared in previous reviews. The paper highlights not only their superior capabilities but also their integration potential, filling a critical gap in current scientific discourse.

1.3. Organization

Section 2 clarifies and updates the main definitions based on recent breakthroughs; this section categorizes, organizes, and reviews existing technologies applicable to noninvasive wearable BCIs, standardizes the definition of "wearable," and further expands the scope of "noninvasive" in the BCI field to better adapt to emerging devices.

Section 3 centers on the ESAD sensors, mainly providing a detailed introduction to the emerging OPM-MEG sensors, organizing literature, analyzing their theoretical and engineering limitations, and proposing directions for future solutions.

Section 4 focuses on BOLD sensors, particularly PAI, and surveys their applications. Given the relatively advanced stage of development of PAI technology compared to OPM-MEG, this section is intentionally

Table 1
Comparison of recent reviews in the field of BCI.

Ref.	Year	General information			ESAD sensors				BOLD sensors		Multimodal		Reuse architecture of new multimodal BCI
		BCI	Wearable	Noninvasive	EEG	OPM-MEG			fNIRS	PAI	Reasons and advantages	Present dilemma	
						Advantage	Theoretical limitation	Engineering limitation					
Zhang et al. (2023)	2023	✓	✓	✓	✓								
Aslam et al. (2023)	2023	✓				✓	✓						
Yang et al. (2021)	2021	✓	✓	✓					✓	✓	✓	✓	
Uchitel et al. (2021)	2021	✓	✓	✓	✓				✓		✓	✓	
Salahuddin and Gao (2021)	2021	✓		✓					✓		✓		
Liu et al. (2021b)	2021	✓		✓	✓				✓		✓	✓	
Liu et al. (2021a)	2021		✓	✓							✓		
Zhuang et al. (2020)	2020	✓		✓	✓								
Shrestha et al. (2020)	2020			✓					✓	✓			
Bai et al. (2020)	2020	✓		✓	✓								
Kumari et al. (2017)	2017	✓	✓								✓	✓	
Udovičić et al. (2016)	2016	✓	✓	✓	✓						✓		
Naseer and Hong (2015)	2015	✓		✓	✓				✓		✓		
Kassab et al. (2015)	2015	✓	✓	✓					✓				
This work	2024	✓	✓	✓	✓	✓	✓	✓	✓	✓	✓	✓	✓

more concise than Section 3 to maintain the focus and coherence of the review, but this does not imply any shift in the relative importance of the two technologies.

Section 5 surveys multimodal BCIs, starting with the reasons for data fusion and the current challenges, proposing the use of light as the core detection medium for multimodal sensor reuse. It also discusses the feasibility of reusing fNIRS and PAI with OPM-MEG and proposes theoretical structures for feasible single/multiple light source MEG-PAI reuse systems to address current challenges in the BCI field.

Finally, Section 6 outlines the future challenges of novel sensor fusion and concludes the work. For convenience, the main content of this paper is outlined in Fig. 1.

2. Wearable and noninvasive BCI

Wearable and noninvasive BCI sensors represent a transformative leap in neurotechnology, offering significant advantages in both research and clinical applications. Noninvasive sensors are designed to

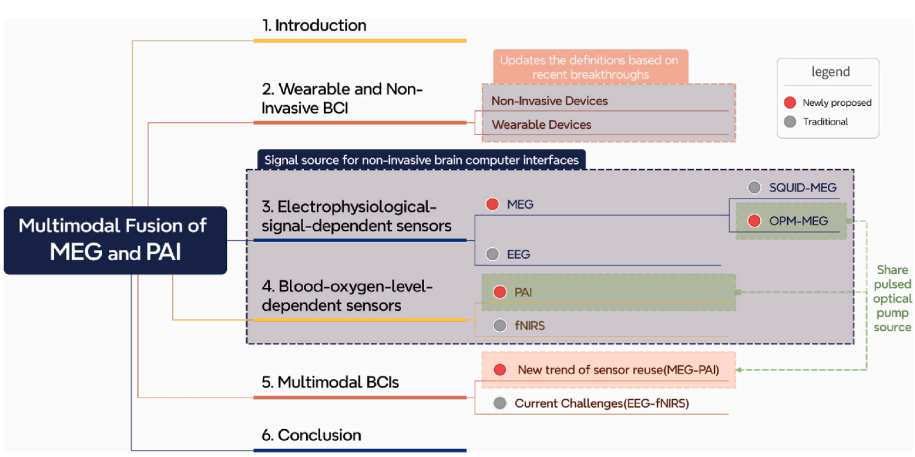

Fig. 1. Framework of this review: BCI: brain–computer interface, OPM: optically pumped magnetometer, SQUID: Superconducting Quantum Interference Device, MEG: magnetoencephalography, PAI: photoacoustic imaging, fNIRS: functional near-infrared spectroscopy, EEG: electroencephalography.

monitor and interpret brain activity without the need for surgical implantation, making them more accessible and less risky for users. However, with the introduction of some new sensors, the limitations of layout or sensor arrangement have been alleviated. Therefore, in Section 2.1.1, we have expanded the traditional definition of "noninvasive BCI." Furthermore, if BCI sensors achieve continuous and real-time monitoring of neural signals in daily environments, they can provide valuable insights into cognitive states, neurological disorders, and human-computer interactions. However, due to current technological limitations, the definition of wearable BCIs remains somewhat ambiguous. Therefore, in Section 2.1.2, we have clarified the definition of "wearable BCI."

Subsequently, in Section 2.2, we discuss the dimensions of BCI, categorizing BCIs into ESAD sensors (Section 2.2.1) and BOLD sensors (Section 2.2.2). We further discuss their sensing theories, limitations, and future development directions.

2.1. Wearable and noninvasive BCI sensors

This section continues from the previous discussion, focusing on new BCI sensors, especially those with the potential to "replace, restore, enhance, supplement, or improve natural CNS outputs." It is important to clarify that this review does not include wearable devices like Google Glasses (Olexa et al., 2024) or fitness bands (Mitro et al., 2023), which, despite their significant roles in assisting surgeries and monitoring vital signs, cannot be classified as BCI devices.

2.1.1. Noninvasive Devices

BCI sensors are primarily categorized into three types based on their mode of acquisition: invasive BCI, semi-invasive BCI, and noninvasive BCI (Rao, 2013). This review focuses on noninvasive BCI sensors, which are typically non-surgical, do not enter the body (Song et al., 2021), and are generally placed outside the scalp (Zhuang et al., 2020). However, with technological progress and innovation in experimental paradigms, some new sensors are designed to be placed in ear (Fig. 2(a) (Kaongoen et al., 2022; Wang et al., 2023)), to reduce the attenuation of signals by scalp or skull, or even in the mouth (Fig. 2(b) (Tierney et al., 2021)) for detecting hippocampal signals. Furthermore, some novel sensors like OPM-MEG have extended paradigms to the spinal cord, enabling non-invasive magnetospinoencephalography for recording cortical evoked responses (Mardell et al., 2024). Although these sensors partially enter the body, they remain nonsurgical and nontraumatic. These methods significantly enhance the application paradigms and efficacy of noninvasive sensing technologies by acquiring more precise biological signals without causing harm to the body. Therefore, in this review, we extend the definition of noninvasive to include nonsurgical and nontraumatic sensors.

2.1.2. Wearable devices

Regarding wearability, most BCI devices still require external wiring for signal transmission or power supply owing to technical limitations. Therefore, the current definition of wearable BCI devices is vague. This paper refers to the general definitions of wearable devices (Ometov et al., 2021; Seneviratne et al., 2017) and considers true wearable BCI devices as those that can independently detect the physiological and environmental data of the user without the need for external wiring for information transmission or power supply. Furthermore, the devices perform data processing and decision-making on cloud or edge platforms, assisting users or being used by users to perform microtasks. It is worth noting that the weight-comfort assessment scales and measurement results for wearable BCI devices are significantly underdeveloped compared to similar virtual reality or headphone devices, even leveraging well-documented weight distribution—approximately 250 g for nasal support, 780 g for ear clamping support, and 1100 g for head support (Møller et al., 1995; Zhuang et al., 2019), theoretically, the total weight of a wearable BCI device, including its direct head connections (e.g., cables), should not exceed 2.13 kg to maintain a reasonable level of comfort. Table 2 compares the advantages and drawbacks of currently available noninvasive BCI devices, and their weights directly connected to the head and whether they exceed 2.13 kg threshold.

For large devices (weighing over 2.l3 kg), X-ray computed tomography (CT) has been commonly used for lesion detection in disease diagnosis. Moreover, combining it with PET or SPECT can improve the specificity and effectiveness of functional imaging (Golan et al., 2020; Russo et al., 2016). Nevertheless, these techniques use ionizing radiation, raising safety concerns with frequent use. To avoid exposure to ionizing radiation, functional magnetic resonance imaging (fMRI) is utilized as a non-ionizing alternative for clinical diagnostics. However, fMRI suffers from low temporal resolution (Lloyd-Fox et al., 2010) and bulky equipment, which limits its suitability for real-time monitoring.

In medium and small-sized devices (with connected parts weighing up to 2.13 kg), optical methods represented by optical coherence tomography (OCT) can be used for high-specificity, high-temporal-resolution detection of blood vessels. However, the limitations of light propagation make it only suitable for small animals (Chen et al., 2016). Ultrasound (US) imaging is used for carotid imaging and stroke analysis because it provides detailed anatomical and hemodynamic information. However, the tissue specificity of the US is relatively low, and ultrasound coupling agents are required to address the impedance mismatch between different media. This tends to limit its feasibility as a wearable device for long-term monitoring (Yang et al., 2021a,b).

Potential noninvasive wearable BCI sensors primarily include EEG (Chen et al., 2014), OPM-MEG (Hill et al., 2022), fNIRS (Chen et al., 2021), and PAI (Yang et al., 2021a,b). A visual comparison of the temporal accuracy, spatial accuracy, mobility, and ease of wearability of these devices is shown in Fig. 3. A detailed comparison of these four different sensing methods is presented in the following sections.

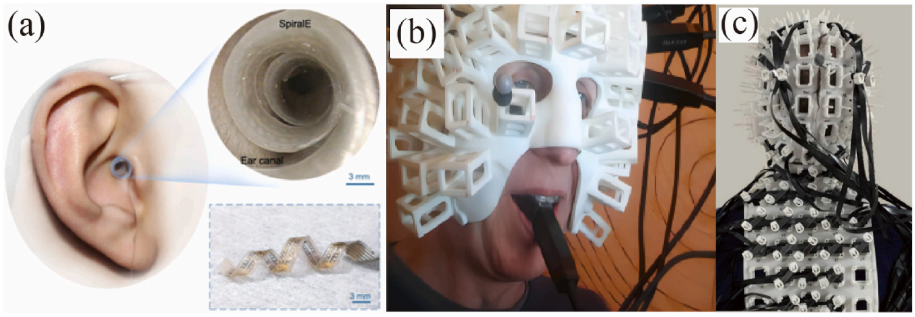

Fig. 2. Extended Definition of Noninvasive Devices: (a) EEG collection in the ear; (b) MEG imaging in the mouth; (c) Noninvasive magnetospinoencephalography cortical evoked responses recording (adapted from refs (Mardell et al., 2024; Tierney et al., 2021; Wang et al., 2023).).

Table 2
Comparison of various noninvasive BCI technologies.

Technology	Imaging Mechanism	Spatial Resolution	Imaging Depth	Equipment Weighing less than 2.13 kg	Ionizing radiation	Ref.
X-ray CT	X-ray absorption	High	Whole-brain	No	Yes	Russo et al. (2016)
PET/SPECT	Positron/photon annihilation	High	Whole-brain	No	Yes	Russo et al. (2016)
MRI	Nuclear magnetic resonance	High	Whole-brain	No	No	Cao et al. (2023)
MEG (SQUID)	Magnetic Induction	High	Below cortical surface	No	No	Weinstock (2012)
MEG (OPM)	Magnetic Induction	Moderate to High	Below cortical surface	Yes	No	Brookes et al. (2022)
US	Ultrasound scattering	Moderate	<3 mm in soft tissue	Yes	No	Zhou et al. (2024)
PAI	Light absorption	Moderate to High	Below cortical surface	Yes	No	Yang et al. (2024b)
EEG	Electroencephalography of brain activity	Low	Below cortical surface	Yes	No	Burle et al. (2015)
fNIRS	Light reflectance	Low	Below cortical surface	Yes	No	Sangani et al. (2015)

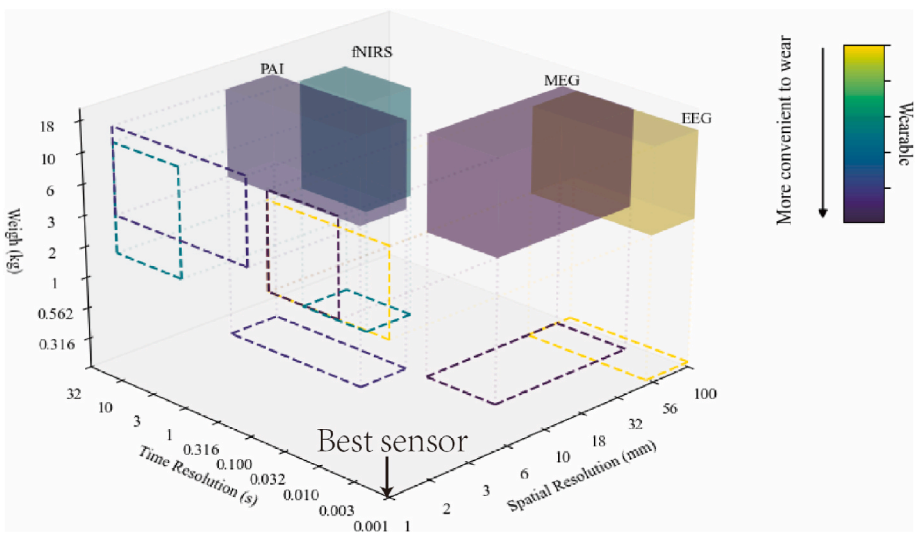

Fig. 3. Overview of temporal and spatial accuracies of various sensing methods.

2.2. Modalities of BCI signals

Noninvasive BCIs can be categorized according to the type of biological signals they detect. Currently, there are two main categories: ESAD sensors (Section 2.2.1) and BOLD sensors (2.2.2).

This section primarily addresses the reasons for these classifications and the corresponding sensing principles. It also introduces the limitations of these sensing types from a theoretical perspective. Notably, to address the shortcomings of single-mode sensing, a multimodal approach that combines these two dimensions of sensors is discussed in detail in Chapter 0.

2.2.1. Electrophysiological-Signal-Activity-Dependent (ESAD) sensors

Observing neuronal electrical activity can be described as "capturing electrophysiological signals produced by the synchronous dendritic currents in a cluster of neurons." Specifically, for the noninvasive capture of neuronal electric/magnetic fields, the neuronal assembly should form a functional entity (neuronal cluster). This is because a sufficiently large group of neurons should gradually operate in a coordinated manner and organize spatially, where the dendrites of multiple neurons generate electrical currents simultaneously. This synchrony can significantly amplify the electrical signals, producing local field potentials (LFPs) and local magnetic fields (LMFs), which are collectively referred to as cortical sources (CSs) of electrophysiological signals, forming the theoretical basis for EEG and MEG signal measurements (da Silva, 2013). According to the measured data, various source localization methods can be employed, such as the classical minimum norm estimation (MNE) (Sarvas, 1987) and its variants, including weighted MNE (Lin et al., 2006) and spatial smoothing constraints MNE (Giraldo-Suarez et al., 2016). Additionally, recent advancements in deep learning and data-driven approaches (Ieracitano et al., 2022) have been increasingly applied to source localization, with several hybrid methods also being proposed.

EEG and MEG are commonly used methods in the neurocognitive field, involving experimental paradigms that mostly deal with event-related potentials or event-related fields (ERFs). These are rapid and relatively short-lived brain activities precisely locked in time with certain cognitive events (Cohen, 1972; Cohen and Cuffin, 1983; Niedermeyer, 2011; Thielen et al., 2015; Verbaarschot et al., 2021), and non-event-related noise can be eliminated, making event-related signals more prominent. This method is applicable to conditions such as consciousness disorders (Huang et al., 2019; Pan et al., 2018; Xie et al., 2018), Parkinson's disease (Kasahara et al., 2018), paralysis (Han et al., 2019; Nicolelis et al., 2022; Verbaarschot et al., 2021), stroke (Lu et al., 2020; Miao et al., 2020; Sebastián-Romagosa et al., 2020), depression (Acharya et al., 2018), autism (Amaral et al., 2018), sleep disorders (Runnova et al., 2021), and even drug addiction detection (Gao et al., 2025). However, cortical electrical signals must traverse multiple layers of tissue with varying electrical properties and complex structures before reaching the scalp. The differing conductivities of the

cerebrospinal fluid, skull, and skin influence the LFP (DEL et al., 2008; Hortal et al., 2015; Yang et al., 2024a) but have less impact on the LMF (Barry et al., 2016). Besides signal distortion before reaching the scalp, the impedance between the scalp and electrodes presents a major challenge for EEG signals, which still depend on wet electrode caps for stable and reliable data collection. However, the conductive gel used in wet electrodes dries over time, resulting in performance degradation and limiting their suitability for long-term EEG recording (Zhang et al., 2023). To address these issues, researchers have developed hydrogel electrodes (Hsieh et al., 2022; Shen et al., 2021), comb-shaped active dry electrodes (Lin et al., 2019; Pourahmad and Mahnam, 2016), and ring-shaped micro-needle dry electrodes (Li et al., 2021). Nevertheless, the contact impedance between dry electrodes and the hairy scalp is generally higher than that for wet electrodes (Zhang et al., 2023). Therefore, attention has turned to MEG devices that do not require a medium for direct skin contact.

Although MEG provides comparable or superior spatial resolution and signal-to-noise ratio (SNR) to EEG (Hansen et al., 2010), it cannot measure radial components. EEG is sensitive to both tangential and radial components of dipole sources owing to its scalar nature, whereas, in theory, radially oriented dipole sources do not generate a magnetic field beyond a spherical volume conductor, making MEG unable to detect these components. Hence, the LMFs can primarily reflect the magnetic fields produced by tangential dipoles (Ahlfors et al., 2010). This involves a discussion of the usefulness of triaxial OPM-MEG sensors and multichannel series disturbances, as detailed in Section 3.3.4.

As technology evolves, OPMs-MEG is considered a BCI technology that blurs the line between "invasive" and "noninvasive." In contrast to EEG, which requires a conductive medium, the OPMs-MEG does not rely on a conductive medium, thus enabling additional flexible sensor placement that is not limited to the scalp. For example, sensors can be placed in locations that are difficult to reach using traditional MEG or EEG technologies, such as the inside of the mouth (Fig. 2(a)). Consequently, this enhances the SNR and effectively captures radial dipole information. Simulation studies have confirmed that the ideal location for detecting magnetic fields in the hippocampus is on top of the oral cavity (Tierney et al., 2021).

2.2.2. Blood-Oxygen-Level-Dependent sensors

The observational requirement for BOLD sensors can be specified as "capturing changes in the regional Cerebral Blood Flow (rCBF) or Cerebral Metabolic Rate of Oxygen ($CMRO_2$) (Roy and Sherrington, 1890) to map neuronal activity." (Adaptation of Hemodynamic-Metabolic Methods, based on a century-old theory by Roy and Sherrington, originally included rCBF, cro2, and regional cerebral glucose metabolism. Here, considering the need to meet the requirements of noninvasive wearable BCIs, the discussion of regional Cerebral Metabolic Rate of Glucose is temporarily omitted.) Specifically, the conditions for noninvasive capture of blood oxygen saturation fluctuations require that neuronal activity in specific brain regions changes significantly and should be sufficiently long to cause detectable hemodynamic responses. Enhanced brain function is associated with rapid increases in oxygen consumption, glucose uptake, metabolism, and blood flow in the activated regions (Filosa, 2010; Sotero and Trujillo-Barreto, 2008). These result in increased local blood flow and oxygen saturation. Blood flow control by small arteries is spatially well-matched with increased neuronal activity, and oxygen demand changes are closely related to electrical changes. The synchrony and locality of the blood oxygen changes can significantly amplify the variations in blood oxygen levels, collectively referred to as cerebral hemodynamic sources (Tomita et al., 1978) forming the theoretical basis for fNIRS (Turner and Jones, 2003) and PAI signal measurements.

Both fNIRS and PAI signals originate from vascular activity; however, their temporal dynamics are poor (~5–8 s) (Horwitz et al., 2000). Specifically, fNIRS measures brain oxygenation by detecting variations in near-infrared light absorption as it passes through the scalp and brain tissue, thereby focusing on changes in blood oxygen saturation (Chai et al., 2024; Turner and Jones, 2003). In contrast, PAI technology employs short laser pulses to excite tissue and images by detecting ultrasonic signals generated by the photothermal effect, providing both blood sample signals and structural and functional information (Chai et al., 2024; Horwitz et al., 2000).

Moreover, owing to the scattering of near-infrared light in tissues, the spatial resolution (2–5 mm) and limited detection depth of fNIRS (Horwitz et al., 2000) make it difficult to provide precise imaging of deep brain tissue. In comparison, PAI offers higher spatial resolution and deeper detection depth, as ultrasound signals emit far less scatter than light waves (~1000 times). This characteristic makes PAI a highly promising technique for deep brain imaging.

3. Novel ESAD sensors — OPM-MEG

In this section, we first review the developmental history of MEG technology. Traditional MEG devices are primarily based on the principles of SQUIDs. Section 3.1 will elaborate on the main differences between SQUID and the emerging Optically Pumped Magnetometers (OPM). Although OPM technology does not require large external equipment or a cryogenic environment like SQUID, some theoretical limitations of OPM pose challenges in research and development, which will be discussed in Section 3.2. Furthermore, designing an OPM as a new type of magnetometer for MEG, attempting to replace the traditional SQUID model, involves several engineering issues, which will be thoroughly examined in Section 3.3.

3.1. MEG devices based on SQUID and OPM

MEG records magnetic fields inside or outside the head to produce 3D images (source localization) that illustrate how LMF change instantaneously in response to different experimental conditions or cognitive demands (Brookes et al., 2022; Cohen, 1972). As shown in Fig. 4, the typical strength of the brain's magnetic field outside the scalp ranges from 10 to 100 fT (1 fT = 10^{-15} T), which is approximately 10^{-9} times that of the Earth's magnetic field. Even though these signals are extremely weak, the MEG systems, which are based on SQUID or OPM theory (Barry et al., 2016; Williamson et al., 2013), have both demonstrated the ability to detect weak brain magnetic signals, even against the backdrop of the Earth's magnetic field and external electromagnetic interference (Presacco et al., 2011).

Based on superconducting Josephson junctions, SQUID emerged as one of the earliest quantum sensor techniques in the 1960s to enable the detection of magnetic fields inside the brain (Weinstock, 2012). SQUIDs have been widely used for geomagnetic and brain magnetic detection, achieving measurement sensitivities of up to 10^{-3} fT/Hz^1/2 in controlled laboratory environments (Simmonds et al., 1979). In practical tests, femtotesla-level (fT) sensitivity can be reached, which is essential for detecting weak magnetic fields produced by the brain. Currently, SQUID-MEG offers millisecond-level temporal resolution and a spatial resolution of approximately 2–5 mm (Bonaiuto et al., 2018), with a CS localization accuracy comparable to that of EEG (Cohen et al., 1990). Many SQUID-MEG sensors are commercially available. However, SQUIDs require a cryogenic environment (Around −269 °C) to maintain superconducting properties (Cohen, 1972; Hämäläinen et al., 1993), necessitating bulky liquid helium dewars for cooling (system weight of approximately 450 kg). In addition, owing to temperature considerations, the sensors must maintain a vacuum gap within the range of 17–30 mm from the scalp for insulation. The attenuation of magnetic signals is proportional to the square of the distance, which is significantly increased in subjects with smaller heads, such as children. This reduces the signal strength and limiting the experimental paradigms. Hence, fixed-position SQUID-MEG systems are cumbersome, as shown in Fig. 5(a).

Since 2002, OPMs, which have similar operating principles to MRI

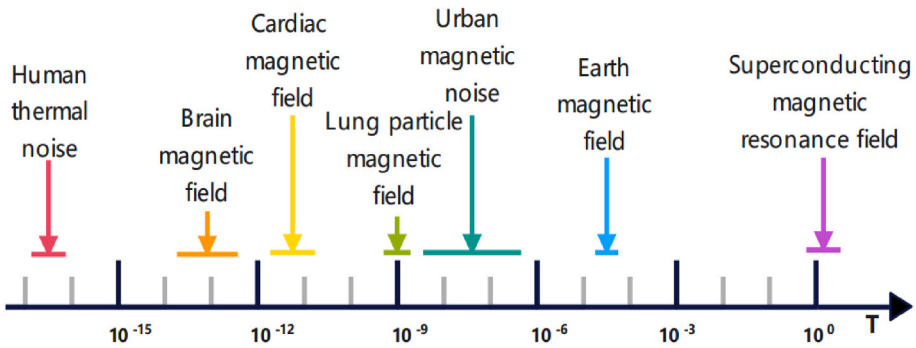

Fig. 4. Magnetic field strength distribution.

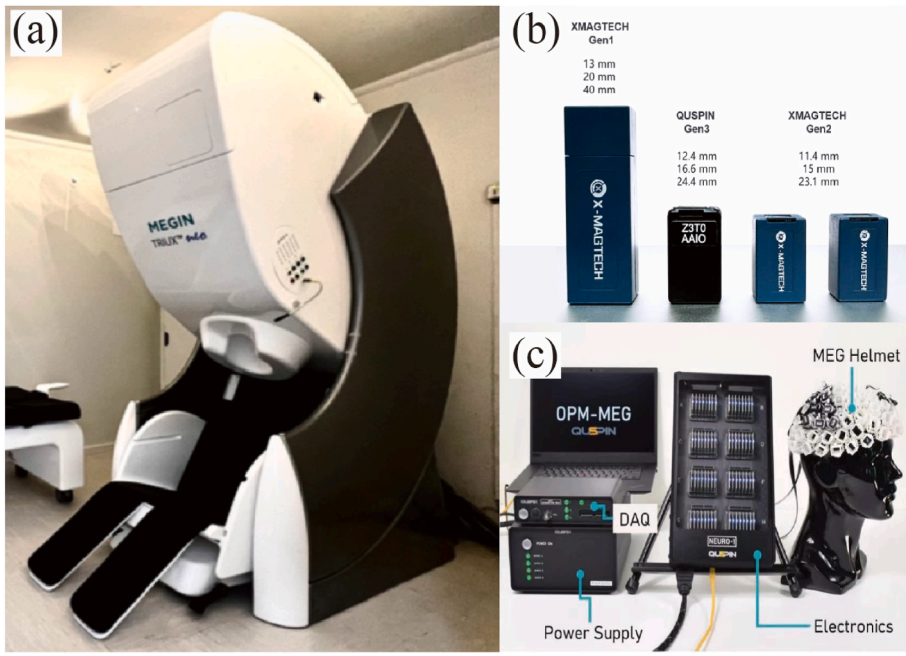

Fig. 5. SQUID-MEG and OPM-MEG systems: (a) SQUID-MEG system (from Zhang Jiang Brain Image Center); (b) Comparison of single-channel sizes of commercial OPM-MEG systems, (c) QuSpin's commercially available third-generation OPM-MEG helmet and external equipment, with a helmet weight of approximately 2 kg. (adapted from ref (Boto et al., 2018).).

and rely on the manipulation of atomic spin properties, have attracted considerable attention (Allred et al., 2002; Kominis et al., 2003). Spin is the basis of particle magnetic moments and their responses to magnetic fields (Tierney et al., 2019). Romalis and Savukov utilized the spin exchange relaxation-free (SERF) phenomenon (Kominis et al., 2003) to effectively reduce the decoherence within the atomic spin system by increasing the temperature, which significantly enhanced the sensitivity of OPM-MEG (~10 fT/Hz^1/2) (Savukov and Romalis, 2005). Fang et al. further studied the effects of coherence loss among atoms at near-room temperatures (Fang et al., 2015). There has been significant development in recent years regarding OPM-based sensors (Allred et al., 2002; Borna et al., 2017; Dupont-Roc et al., 1969; Kominis et al., 2003; Shah et al., 2007; Shah and Wakai, 2013), which are considered highly suitable for MEG measurements (Alem et al., 2014; Alem et al., 2017; Boto et al., 2017; Johnson et al., 2010; Johnson et al., 2013; Kamada et al., 2015; Kim et al., 2014). In 2018, Boto et al. applied OPM technology to wearable MEG devices (Boto et al., 2018) and achieved precise brain activity measurements, as shown in Fig. 5(b). Compared with SQUID devices that require liquid helium cooling systems, OPM technology does not require expensive cooling systems, significantly reducing the operational and maintenance costs of the equipment and allowing sensors to be positioned closer to the subject's brain. This advantage enhances sensitivity to CSs and ensures consistency across varying head shapes and sizes, which can differ by factors of 3–5 (Boto et al., 2016; Iivanainen et al., 2017). Although the precision in a laboratory environment is 10 times lower than that of SQUIDs, subjects wearing sensors can perform tasks and move relatively during brain activity recordings (Aslam et al., 2023).

The core of an OPM typically consists of a chamber filled with a vapor containing ^{87}Rb (Boto et al., 2018) or ^{4}He (Gutteling et al., 2023) atoms. The magnetic moments of the Rb atoms are randomly oriented in the absence of an external magnetic field. However, when a beam of circularly polarized light at 795 nm (tuned to the D1 transition of Rb) is introduced to polarize the atomic spins, the atoms continuously absorb photons until their spin magnetic moments align with those of the laser beam. In this state, the atoms cannot absorb additional photons, rendering the vapor transparent to the laser and maximizing the light detected by the photodiode at the backend. This phenomenon is known as the "zero-field resonance."

When the chamber is affected by varying magnetic fields, such as those emanating from the brain, a magnetic dipole's moment in the magnetic field, B, experiences not a force but a torque given by:

$$\vec{\tau} = \vec{\mu} \times \vec{B} = -\gamma \vec{S} \times B = \frac{d\vec{S}}{dt}, \quad (1)$$

From this, the external magnetic field causes the atoms to precess at the Larmor frequency $\omega_L = |\gamma B|$, where γ is the gyromagnetic ratio of the atom, reducing the net alignment of the magnetic moments, which allows the atoms to absorb light again. By detecting changes in light polarization, the magnetic field can be measured, which is the principle of a non-polarization-modulated single-beam OPM, also used in most early commercial sensors for magnetic field detection (Boto et al., 2022; Dupont-Roc et al., 1969; Savukov et al., 2017) (as seen in Gen1 and Gen2 in Fig. 5(b)). Recently, new commercial sensors have been introduced in a three-axis form (Gen3 in Fig. 5(b) and the system composed of three-axis sensors in Fig. 5(c)) but the benefits, frequency effects, and the associated multi-channel series disturbances brought by multiple axes are worth discussing, as detailed in 3.3.4.

Table 3 presents a comparison of devices from previous studies, and the trend analysis suggests that, since its (Kominis et al., 2003) initial design already achieved precision levels nearly comparable to SQUID, the current development directions focus primarily on miniaturization (Fang et al., 2014; Griffith et al., 2010; Johnson et al., 2010; Schwindt et al., 2004), multi-channel integration (Johnson et al., 2010; Kim et al., 2014; Li et al., 2006; Wyllie et al., 2012), cryogenic or room-temperature operation (Fang et al., 2015; Gerginov et al., 2017; Ledbetter et al., 2008), and unshielded designs (Limes et al., 2020; Zhang et al., 2020).

3.2. OPM-MEG's theoretical limitations and solutions

In the theory of OPM-MEG, relaxation time is the most significant factor influencing performance. It can be conveniently adjusted by modifying the atomic density or the volume of the cell, but the relaxation time simultaneously affects the balance between sensitivity and response bandwidth (Tierney et al., 2019). To reduce 1/f noise and meet the requirements of multi-axis vector detection, current methods typically add an oscillating magnetic field at a certain frequency. The original magnetic field value is then obtained using a phase-locked loop, which further introduces nonlinearity into the sensor. Therefore, the current focus of theoretical research is on how to enhance sensitivity without adversely affecting nonlinearity and response frequency.

3.2.1. Relaxation effects and sensitivity

The biggest issue with OPM devices developed based on microscopic theories at the macroscopic scale is relaxation, arising from (1) spin-exchange collisions among atoms leading to polarization loss R_{se}, (2) spin-destructive collisions between atoms or with other molecules causing depolarization R_{sd}, and (3) collisions of atoms with the walls of the gas chamber R_{wall} (Allred et al., 2002; Kornack, 2005). According to the sensitivity formula (Ledbetter et al., 2008):

$$\delta B = \frac{1}{\gamma\sqrt{n\tau V t}}, \quad (2)$$

where n denotes the atomic number density, V is the effective volume used in measurements, and t is the measurement time. The primary limiting parameter for sensitivity is the relaxation time τ (Kominis et al., 2003; Purcell and Field, 1956). To mitigate this limitation, the vapor is heated to approximately 150 °C to reduce coherence loss owing to atomic collisions (Boto et al., 2018). Furthermore, when atoms are in the SERF state, considering precession, pumping, and relaxation effects together, the macroscopic description of the atomic spins evolving in a magnetic field using the Bloch equations can be simplified to the SERF state OPM formula:

$$\frac{dS}{dt} = \gamma S \times B + \frac{1}{\tau}(S_0\hat{x} - S) \quad (3)$$

Equation (2) precession term $\gamma S \times B$ describes the precession motion of the magnetization vector S under the spin vector B, where the relaxation term $\frac{1}{\tau}(S_0\hat{x} - S)$ describes the relaxation process of the

Table 3
Representative OPM-MEG studies with different atoms and cell temperatures.

Year	Affiliations	Gas Cell Material	Temperature (°C)	Accuracy (fT/Hz^1/2)	Require shielded	Peculiarities	Ref.
2003	Princeton University	K	180	0.54	Yes,room	Achieved 2 mm magnetic field source localization	Kominis et al. (2003)
2004	NIST	Rb	152	70	/	Fabricated using MEMS technology	Schwindt et al. (2004)
2006	University of Wisconsin-Madison	Rb	188	60	Yes, bucket	Conducted a 20-channel experiment and compared results with a 306-channel SQUID-MEG system	Li et al. (2006)
2008	University of California, Berkeley	Cs	103	40	Yes, bucket	Introduced the use of uncommon elements to achieve lower operating temperatures	Ledbetter et al. (2008)
2010	NIST	Rb	200	5	Yes, bucket	Developed a 1 mm^3 cell via silicon wafer etching, ensuring accuracy	Griffith et al. (2010)
2010	Princeton University	K	200	0.16	Yes, bucket	Assessed magnetometer performance under ultra-high temperature conditions (420 °C)	Dang et al. (2010)
2010	NIST	Rb	190	5	Yes, bucket	Employed two different wavelengths for optical pumping and detection	Johnson et al. (201))
2012	University of Wisconsin-Madison	Rb	158–170	6–11	Yes, bucket	Developed a modular design with fiber coupling for array configurations	Wyllie et al. (2012)
2014	Korea Institute of Standards Science	K	200	4	Yes, bucket	Conducted source localization of auditory evoked fields using equivalent current dipoles	Kim et al. (2014)
2014	Beihang University	K-Rb	195	5	Yes, bucket	Optimized an OPM using a mixture of two alkali metal elements	Fang et al. (2014)
2015	Beihang University	Cs	85	55	Yes, bucket	Reported on a very low temperature project	Fang et al. (2015)
2017	NIST	Rb	85	300	Yes	Investigated pulsed light sources in very low temperature environments	Gerginov et al. (2017))
2020	Princeton University	Rb	100	16	No	Conducted an unshielded, very low temperature experiment	Limes et al. (2020)
2020	Peking University	Cs	~25	4	No	Conducted an unshielded, room-temperature experiment	Zhang et al. (2020)
2022	Peking University	Rb	150	/	Yes, bucket	Investigated multimodal fusion techniques	Ru et al. (2022)

K: Potassium; Rb: Rubidium; Cs: Cesium; NIST: Time and Frequency Division National Institute of Standards and Technology; MEMS: microelectromechanical systems technology.

magnetization vector S toward the equilibrium state $S_0\hat{x}$, where τ denotes the relaxation time and, S_0 is the spin polarization when there is no magnetic field and pumping and relaxation are balanced.

3.2.2. Balance of sensitivity, response nonlinearity, and response bandwidth in OPM systems

By reducing the relaxation time, the system becomes highly sensitive to small magnetic field changes, but it also becomes susceptible to low-frequency 1/f noise (Osborne et al., 2018). One effective solution is to modulate the amplitude of the polarization and employ lock-in detection technology to measure this modulation. According to the theories proposed by Rev et al. (Cohen-Tannoudji et al., 1970), by applying two modulation fields that are phase- or frequency-separated, magnetic fields in two directions perpendicular to the beam can be measured simultaneously. Thus, frequency modulation is commonly used in the OPM field, adding modulation magnetic fields at frequencies ω_x and ω_z, and in the presence of an external magnetic field $|B| \ll \Delta B$, the optical pumping response in the X-axis direction can be derived from equation (3):

$$S_x = \frac{S_0}{\Delta B^2}\left[\Delta B B_y + B_{x0}B_{z0} + B_{x0}B_z^m \cos(\omega_z t) + B_{z0}B_x^m \cos(\omega_x t)\right]$$

$$+\frac{S_0}{\Delta B^2}\left[B_x^m B_z^m \cos\left(\omega_x + \omega_z\right)t + B_x^m B_z^m \cos\left(\omega_x - \omega_z\right)t\right] \quad (4)$$

Therefore, OPM-MEG can employ a lock-in amplifier to demodulate the output signal for frequency components ω_x and ω_z to obtain the bias fields B_z and B_x. After establishing a feedback compensation mechanism, the DC component of the output signal is only proportional to B_y. Thus, the three-axis magnetic field vectors can be demodulated from the components of the output signal, using this beam for both pumping and detection (Sun et al., 2023).

The steady-state solution of the macroscopic equation (4) illustrates the combined effect of optical pumping and magnetic fields on polarization. Polarization along the laser axis (Px) showing an absorption curve, while the polarization along another axis (Py) has a dispersive shape.

Due to its dispersive curve characteristics, the sensor can distinguish between positive and negative magnetic field changes, classifying it as a "vector" magnetometer. However, this also implies that the system's response to a broad range of magnetic field changes is nonlinear. For instance, if a sensor's dynamic range is ±1.5 nT, the response curve yields a deviation of <1% at 1 nT. However, significant nonlinearities are introduced in the response when the sensor encounters larger magnetic fields (>15 nT) (Tierney et al., 2019), shown in Fig. 6.

Increasing the relaxation time τ to enhance sensitivity also steepens the response curve, thereby narrowing the linear range (see Fig. 7). Additionally, as τ is a time constant that determines the interval required before another independent measurement can be performed, increasing τ results in a reduction of the measurement bandwidth. Consequently, a balance must be struck between sensitivity, nonlinearity, and response bandwidth. Presently, the response frequency of continuous-wave miniaturized OPM-MEG systems is limited to around 100 Hz (Tang et al., 2021; Tierney et al., 2019). A significant advancement was made with the introduction of pulsed pump light sources. Tang et al. achieved an accuracy of 60 fT/$\sqrt{\text{Hz}}$ at 10 kHz using pulsed pump sources (Tang et al., 2022). However, the complexity of this optical design introduces challenges for miniaturization.

3.3. Engineering limitations and current solutions for OPM-MEG

Beyond the theoretical challenges of balancing sensitivity, response nonlinearity, and bandwidth, practical engineering applications encounter numerous issues not faced by traditional noninvasive sensors like Temperature and Flex Cap Registration Issues in 3.3.1, Improvements in "10–20" System Placement in 3.3.1, External Magnetic Shielding and Dynamic Range Saturation Issues in 3.3.3, or Device Crosstalk and Development of Multi-Axis Sensors in 3.3.4.

3.3.1. Temperature and Flex Cap Registration Issues

"EEG-like" flex caps facilitate flexible sensor array arrangements, enabling sensors to be positioned closer to the scalp. Furthermore, the arrangements reduce the possibility of heat accumulation for sensors in enclosed spaces, which helps convect heat away from the head. To address the decoherence effects within the ^{87}Rb atomic spin system, commercially available devices heat the atomic chambers to above 100 °C, for example, the 150 °C used by QuSpin devices, as shown in Fig. 5(c).

Therefore, the chambers should be offset from the sensor's outer walls to increase the distance from the brain (~4–6 mm), ensuring that the external temperatures of the sensors do not exceed approximately 40 °C. Importantly, when using different vapors, such as ^{4}He, heating is not required; however, this results in reduced sensitivity (Fourcault et al., 2021; Labyt et al., 2018). In contrast, by using more channels in ^{87}Rb-based OPM-MEG systems, the additional heat might cause discomfort for participants, necessitating active cooling (e.g., air or water) in future OPM-MEG systems (Pang et al., 2022a).

Owing to the vector nature of sensors, there is an increased demand for precise collection of positions and sensor pitch angles. Existing registration methods primarily use structured light scanning (Boto et al., 2018; Cao et al., 2023) and the iterative closest point (ICP) algorithm to

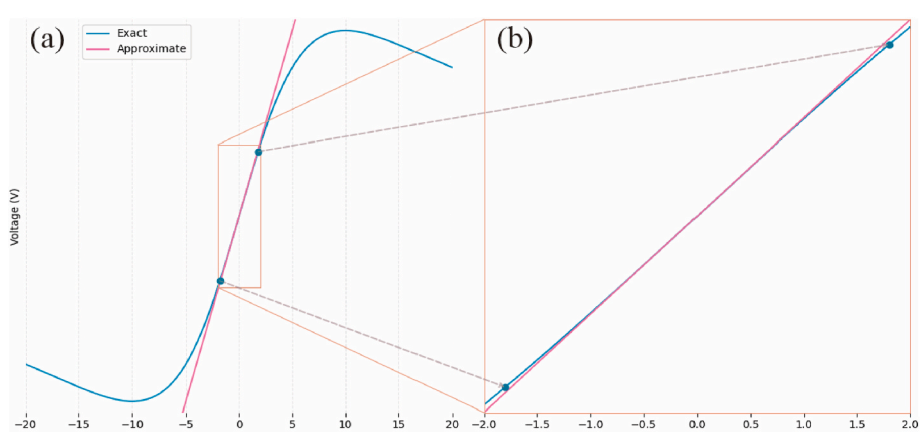

Fig. 6. Response curve and nonlinearity issues within a ±1.5 nT dynamic range: (a) Nonlinearity issues must be considered when dealing with data over a large processing range. (b) Enlarged view of the boxed area: When examining the curve within the sensor's dynamic range (±1.5 nT), the linear approximation of the curve produces less than 1% deviation at 1 nT.

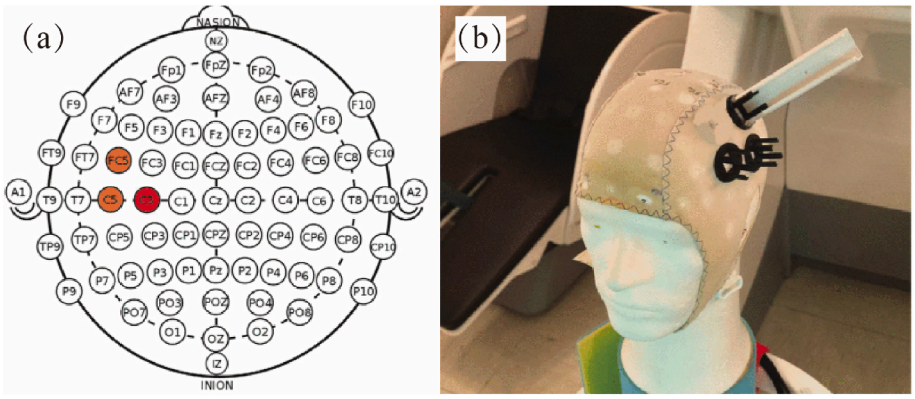

Fig. 7. MEG system sensor positioning diagram: (a) three sensors positioned in direct contact with the scalp; (b) reference sensor positioned 7 cm above the C3 sensor (adapted from ref. (Fedosov et al., 2021)).

determine the position and orientation of the sensors precisely. The average co-registration position error for all the sensors is close to 1 mm, whereas Cao et al. accomplished an average positioning error of less than 2.5° in the X and Y directions and less than 1.6° in the Z direction (Cao et al., 2023).

3.3.2. Optimization of OPM-MEG sensor placement within "10–20" system framework

The new sensor theory implies that the arrangement suited for its data collection may not be directly compatible with the "10–20" system. Initially, wearable OPM-MEG sensors were designed using anatomical MRI scans of subjects [98]. Newer studies have shown that the minimal system unit might be simpler than the EEG using the "10–20" template. For example, a previous OPM-MEG study (Fedosov et al., 2021) achieved hand movement imagery with an 8-channel setup (three sensors close to the scalp + one sensor further from the scalp, with each sensor detecting both radial and tangential axes). Further, they attempted to reduce the number of channels to two, concluding that a single sensor located at the C3 or C5 position of the "10–20" template (2 channels) achieved nearly equivalent binary classification accuracy compared to a combined analysis of C3-C5-FC5-ref (8 channels). This suggests that OPM-MEG sensors can potentially simplify equipment and enhance operational convenience by reducing the number of sensors without significantly compromising performance. Future research should further explore and optimize the sensor arrangement to enhance the efficiency and practicality of BCI systems.

3.3.3. External Magnetic Shielding and Dynamic Range Saturation Issues

Owing to its nonlinearity limitations, the current OPM-MEG equipment is easily overwhelmed by its suitable dynamic range. The reasons for this include the vector nature of the data structures and external magnetic field disturbances. The vector nature means that relative movements against a constant magnetic field can also cause fluctuations that potentially exceed the dynamic range of the sensor. For example, in a "typical" OPM-MEG shielding environment (background field of ~30 nT), a head rotation of 4° can push an OPM beyond its dynamic range (+5 nT), making it inoperable. However, even with head movements, wearable systems can still collect high-fidelity data with spatial resolution and robustness superior to those of SQUID-MEG (Brookes et al., 2022).

Regarding the external magnetic field interference, the dynamic range of the OPM-MEG is significantly limited, which restricts its operation to weak magnetic environments of approximately 10 nT or less (primarily within zero magnetic environments inside the shielding cylinders). Magnetic shielding devices are often impractical for many applications where the test subject is significantly large or the external magnetic field fluctuations far exceed 10 nT during testing. For example, in geoscience (~50,000 nT), magnetic shielding completely blocks signal measurements. A simpler example is the movement of BCI users, which may be influenced by changes in the Earth's magnetic field, posing a challenge to the accuracy of MEG data. Because changes in the Earth's magnetic field may mix with the magnetic field signals produced by brain activity, real-time correction of these external magnetic interferences is necessary. This generally requires advanced magnetic field correction methods, such as monitoring the environmental magnetic field changes using reference magnetic field sensors and removing these disturbances from the MEG data through algorithms. This real-time correction technology is crucial for maintaining the reliability and accuracy of the data, particularly when measuring complex or dynamic environments.

To address the shielding problem, Romalis et al. pioneered research on unshielded OPM sensors in 2004 (Seltzer and Romalis, 2004). However, the system response bandwidth was approximately 10 Hz, and the magnetic noise cancellation effect was poor, ultimately achieving only 1 pT/Hz^1/2 sensitivity. By 2017, Sheng et al. achieved a uniaxial sensitivity of 0.5 pT/Hz^1/2 (Sheng et al., 2017), and by 2020, Twinleaf's Limes, in collaboration with Romalis's research team, developed a portable gradient magnetic probe (Limes et al., 2020), achieving a gradient sensitivity of 16 fT/Hz^1/2 in field geomagnetic environments, and successfully measuring human brain magnetic signals in unshielded conditions.

3.3.4. Device Crosstalk and Development of Multi-axis sensors

Whether it is multi-axis modulation to measure multi-axis magnetic fields or shielding external magnetic fields, nearby sensors can be affected because the amplitude of the modulation fields maybe 50–100 nT, whereas the magnitude of the DC bias zero fields maybe 2–50 nT. As more complex multi-axis sensors have been developed, serial disturbances may become more severe compared to single-axis sensors (Brookes et al., 2021). To date, no experiments involving three-axis sensors have been reported.

Additionally, as discussed in 2.2.1, if the object being detected (human brain) lacks radial components, whether it is worthwhile to perform three-axis measurements in OPM-MEG has been debated. Theory (Sarvas, 1987) suggests that the head can be assumed to be a spherical homogeneous conductor with a current-free extracranial space, given that the radial field components at all points on the conductor's surface are known. This assumption can be used to derive the local magnetic scalar potential. Subsequently, the scalar potential can be used to derive the 3D vector field. Therefore, apart from the information obtained from the radial fields alone, independent measurements of the tangential field components do not provide additional information; hence, theoretically, the value of the three-axis measurements is limited.

However, in practical MEG experiments, adding three-axis measurements has three theoretical impacts (or advantages):

1) Limited spatial sampling implies that we do not know the radial field at all locations, resulting in gaps in sensitivity to potential sources, particularly for shallow currents beneath the radial sensors. Three-axis measurements can fill these gaps.
2) Not all magnetic fields originate within the brain; interference from other sources (e.g., biological, environmental, or cross-sensor disturbances) will be detected, which can be better characterized (and ultimately eliminated) via three-axis rather than radial measurements (Brookes et al., 2021).
3) As shown in Fig. 2(a), measurement points in non-traditional locations (such as the oral cavity) enable in-body measurements, bringing new axial measurement requirements (Tierney et al., 2021).

4. Novel BOLD sensors — introduction to PAI

The photoacoustic (PA) effect was discovered by Alexander G. Bell in 1880 (Wang and Wu, 2007).With advancements in lasers, ultrasonic transducers, and computer technology, PAI has been explored for decades based on the PA effect. Fig. 8(a) illustrates the principle of PAI. The PA effect typically begins when pulsed light strikes the target tissue, and the energy of the photons is absorbed by molecules within the tissue (Step 1). The energy is converted to heat, leading to a transient increase in temperature. Owing to the thermoelastic expansion, the pressure within the tissue increases (Step 2). This pressure propagates in the form of photoacoustic waves, which are detected by ultrasonic sensors (Step 3). Finally, photoacoustic images are obtained through computer calculations based on signal processing and image reconstruction (Step 4). (Yang et al., 2024b).

PAI technology combines the advantages of optical and ultrasonic technologies, providing high resolution, specificity, and excellent penetration depth (Pang et al., 2022b). It is a relatively new non-ionizing radiation medical imaging method. Compared with traditional optical imaging methods such as fNIRS, PAI also provides rich biochemical information. Molecules with strong absorption in biological tissues, such as hemoglobin (Guggenheim et al., 2015), melanin (Longo et al., 2017), and lipids (Guggenheim et al., 2015), are endogenous targets for PAI (Zheng et al., 2022). Recent research on small animals and even human brain microvasculature has demonstrated the potential of PAI for detecting brain injuries (Bodea and Westmeyer, 2021), supporting its application in brain imaging. Many researchers in BCI are leveraging the combined benefits of optical specificity and acoustic penetration from PAI to bridge the gap between resolution and penetration depth in brain imaging (Yang et al., 2021a,b).

Currently, photoacoustic imaging technology faces numerous challenges in practical applications. Beyond simple obstructions such as the skull, gray matter, and white matter that can affect imaging clarity (Yang et al., 2021), interface impedance matching is the most significant factor (Chai et al., 2024). As sound waves propagate through different media (such as skin, air, or sensors within devices), impedance mismatches can cause wave reflections and signal attenuation, impacting image quality. To address this issue, specific ultrasonic coupling agents or new sensor materials and designs are typically needed to improve the efficiency of sound transmission and image clarity. Recent innovations such as flexible ultrasonic sensors (Zhou et al., 2024) and injectable ultrasonic sensors (Tang et al., 2024) have made significant contributions to solving the problem of interface impedance matching. However, further research and development are needed to address artifacts caused by impedance issues in internal cavity organs like the ear canal or esophagus ((Yang et al., 2025)).

Additionally, the miniaturization of imaging interfaces and time constraints limit the development of wearable photoacoustic devices for human use. Due to significant variations in human skin thickness, color, and the depth of internal vascular networks (Waller and Maibach, 2005), miniaturized PAI systems must have adjustable focus capabilities Fig. 8(b). A breakthrough occurred in the present study with the wearable PAI watch developed by Zhang et al., (2024), featuring adjustable focal planes, which weighs only 40 g and uses micro stepper motors to adjust the focal plane as shown in Fig. 8(c).

However, despite this advancement, the imaging speed does not meet the time requirements for BCI applications. PAI commonly employs two imaging modes: the scanning mode and matrix detection mode. In the single-point scanning mode used in miniaturized systems

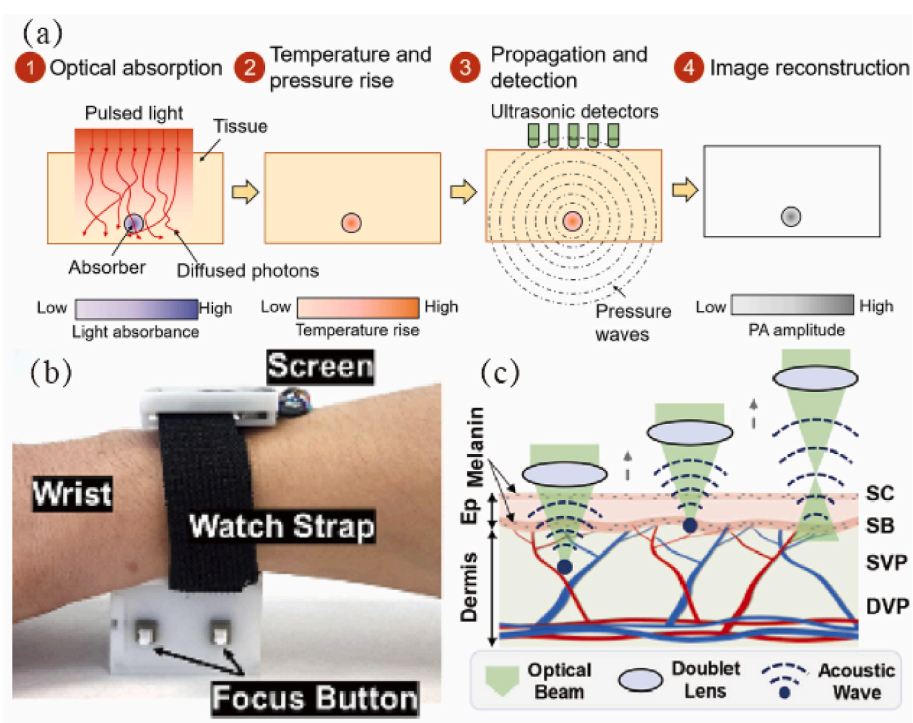

Fig. 8. Principle and practical application of PAI: (a) Schematic of the PAI principle; (b) schematic showing light excitation and sound wave production in multi-layered skin with adjustment of the focus of the light beam; and (c) an actual PAI based watch (adapted from refs (Yang et al., 2021a,b; Zhang et al., 2024).).

such as the one described in (Zhang et al., 2024), even with a light source operating at a maximum repetition rate of 2.5 kHz, capturing a single 500 × 500 pixel image takes 100 s. For precise brain imaging, we typically use the matrix detection mode, which employs 128 or more ultrasound array sensors (Yang et al., 2024a). However, this introduces new challenges related to the complexity and portability of such systems.

5. Current challenges and perspectives of multimodal BCI

In the field of noninvasive BCIs, multimodal data fusion is becoming increasingly popular. This approach aims to integrate the advantages of different measurement technologies to provide more comprehensive monitoring of brain activity. Multimodal BCIs integrate these technologies, aiming to deliver a more comprehensive understanding of brain activity. This section will explore the motivations and current challenges in Section 5.1, and future research directions of multimodal BCI in Section 5.2.

It is important to clarify that, following the discussion in Section 2.1.2, this review does not consider any data fusion involving medium to large equipment, such as PAI with ultrasound (Wang et al., 2016) or MRI (Ni et al. 2018a, 2018b). Therefore, the focus is solely on combinations of EEG, fNIRS, OPM-MEG, and PAI.

5.1. Reasons for choosing multimodal data fusion and current challenges

Among the combinations of two sensors, the most representative is selecting one sensor based on neuronal electrical activity and one based on blood oxygen changes. These combinations can simultaneously measure the electrophysiological and hemodynamic activity in the brain, providing rapid and dynamic information as well as precise blood oxygen and spatial localization. This holds potential value for studying the substrates and mechanisms of neurovascular coupling in both healthy individuals and patients with conditions such as hypertension, Alzheimer's disease, and ischemic stroke (Girouard and Iadecola, 2006; Uchitel et al., 2021).

Before the advent of OPM-MEG, because both EEG and fNIRS are designed to support and accelerate clinical translational research in hospitals and small clinics, emphasizing low cost, portability, and suitability for long-term monitoring of subjects in both clinical or even non-clinical settings (Fang et al., 2022; Uchitel et al., 2021), BCI device research often employed combined EEG-fNIRS systems to enhance the information dimensionality and increase classification accuracy (Casson, 2019; Li et al., 2017). EEG-fNIRS has been proven applicable for conditions like stroke (Li et al., 2020a), Parkinson's disease (Abtahi et al., 2020), and epilepsy (Sirpal et al., 2019). Among other fusion projects, Xi (Xi et al., 2017) and Wang (Wang et al., 2014) completed an EEG-PAI fusion project in rats, while there have been few projects fusing SQUID-MEG with fNIRS till 2024 (Marhl et al., 2024). However, it is noteworthy that after the introduction of OPM-MEG, Ru et al. completed a fusion of MEG-EEG-fNIRS, proving the feasibility of simultaneously measuring brain electrophysiology and hemodynamic responses with these modalities (Ru et al., 2022) (Fig. 9).

Although there have been a large number of multimodal BCI projects (Liu et al., 2021b; Uchitel et al., 2021), the combination of several completely discrete systems presents several major challenges (Xi et al., 2017):

(1) Spatial Synchronization

In multimodal BCI applications, traditional devices such as EEG and fNIRS use wearable soft caps to collect data (Kassab et al., 2015). However, owing to the fundamental differences in their physical construction and functional principles, it is challenging to share sensors or measurement points in the same setup. Bulky fNIRS fibers, EEG cables, and electrodes compete for space on the head (Ahn and Jun 2017), posing mechanical and structural challenges when coupling EEG electrodes with fNIRS light sources and detectors.

(2) Temporal Synchronization

Ensuring sufficient temporal precision and synchronization for simultaneous fNIRS and EEG recordings is challenging (Uchitel et al., 2021). Common solutions include aligning timestamps, using a central synchronization control system, and sharing certain hardware components. Aligning timestamps ensures that data collected from different devices can be precisely matched on a timeline, whereas a central synchronization control system starts all measurement devices at the same time through a unified trigger mechanism to ensure synchronous data collection.

(3) Inter-device Crosstalk

Customized EEG sensors composed of Ag/AgCl powder sintered into

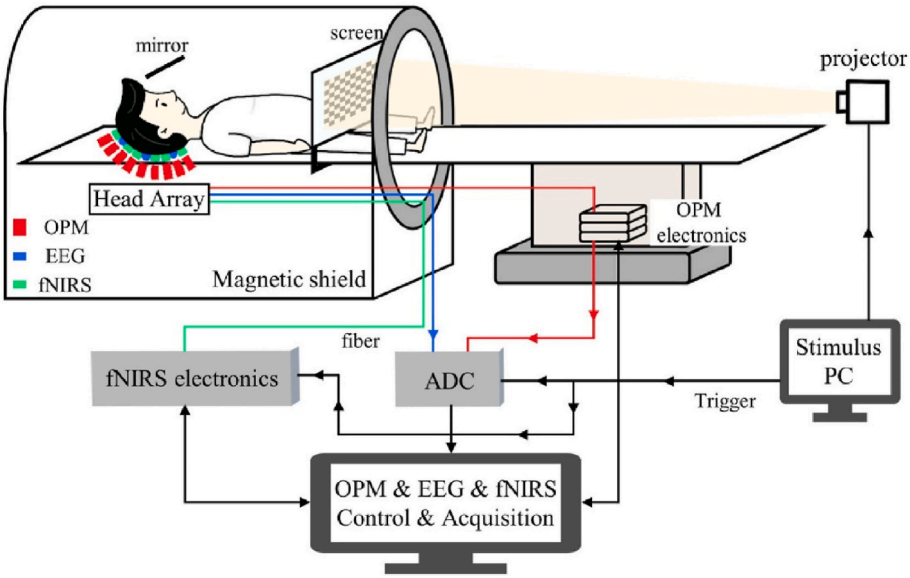

Fig. 9. Structure of EEG-EMG-fNIRS three-mode fusion. (adapted from refs (Ru et al., 2022).).

silver-plated copper wire are required to ensure that the residual magnetic fields they generate are below 50 pT and do not cause changes in the power spectral density of the OPMs (Ru et al., 2022). It is also necessary to ensure that the frequency reuse of high-channel-count light systems does not cause electrical interference with EEG (von Lühmann and Müller, 2017).

5.2. Feasibility of using light as a core medium for multimodal sensor reuse

Noninvasive BCI sensors based on neuronal electrical activity include EEG and OPM-MEG, whereas BOLD sensors include fNIRS and its emerging alternative, PAI. Because OPM-MEG uses OP technology that can produce laser light, it has a natural potential for reuse with BOLD sensors such as fNIRS and PAI, which also require a light source. We describe in this section both theoretical and structural perspectives on the feasibility of sharing light sources between OPM-MEG's optically pumped technology and BOLD sensors.

5.2.1. Reasons why OPM-MEG and fNIRS cannot share light sources

Although OPM-MEG and fNIRS use light sources, fNIRS cannot share its light source with OPM-MEG because fNIRS light sources must be activated according to a precise timing sequence to avoid signal interference between different light sources (Zhou et al., 2020). Moreover, this time-division multiplexing technique requires strict timing control for the activation and deactivation of each light source. fNIRS relies on detecting how light is scattered and absorbed by the brain tissue, which is highly sensitive to the timing of light source activation. If not properly managed, this can lead to data capture errors and affect the accuracy of the experimental results (Li et al., 2020b).

Therefore, although fNIRS provides benefits such as low equipment cost and ease of operation, its application in advanced brain function imaging is constrained by its limited spatial resolution and detection depth, as well as the high demand for light source timing control. These limitations render it impractical for fNIRS to share equipment with a more technologically complex OPM-MEG. This timing is a significant barrier to the application of fNIRS in multimodal brain imaging.

5.2.2. Reasons why OPM-MEG and PAI can share light sources

5.2.2.1. Theoretical basis for sharing light sources between OPM-MEG and PAI. Regarding the wavelength of light, most modern atomic magnetometers, particularly those with significant pressure broadening such as SERF atomic magnetometers (Kornack, 2005), use laser light with a linewidth much narrower than the atomic D1 and D2 transitions. Thus, incident light can be considered monochromatic and suitable for PAI because its purity can enhance the image quality. In addition, unlike fNIRS, PAI detects ultrasonic signals triggered by light pulses, and to enhance these signals, additional light sources may be required to strengthen the photoacoustic response. Thus, PAI can use multiple light sources to improve imaging speed and spatial resolution without strict timing constraints.

However, a major challenge for the technological reuse of OPM-MEG with PAI is that the traditional Bell-Bloom scheme proposed by Bell and Bloom in the 1970s (Bell and Bloom, 1961) relies on a continuous laser source to maintain stable atomic polarization, whereas PAI requires pulsed lasers to generate sufficient energy density for thermoelastic expansion. Although the wavelengths of the two techniques may overlap, their modes of light source usage differ significantly.

Nevertheless, in 2017 Gerginov et al. found that designing the light source in the magnetometer as pulsed improved performance, with performance improving as the duty cycle shortened and peaking at a 1.25% duty cycle (Gerginov et al., 2017). In the same year, Zhang et al. from Peking University used closed-loop feedback to modulate the pump light frequency and track the Larmor precession frequency. Thereby they achieved an extremely high common-mode noise suppression ratio for differential signals (Zhang et al., 2020). Subsequent studies also extended the dynamic measurement range (Borna et al., 2018) and frequency (Tang et al., 2021) of OPM-MEGs using pulsed lasers. This has significantly expanded the potential for OPM-MEGs to be adapted for PAI.

In summary, for a single-light source system of OPM-MEG and PAI, the key is to ensure that a single pulse can complete a full relaxation process with the pump light source. In addition, by adding a beam splitter (BS) to guide another beam, sufficient initial acoustic pressure waves can be generated to enable the ultrasonic probe of the PAI system to capture signals. For multilight source systems, the current system's 500-μW average power light source can produce 10.2 nJ of energy per pulse without modifying the existing pump structure (Gerginov et al., 2017) according to the photoacoustic-effect formula:

$$p(t,\boldsymbol{r}) = \Gamma \int_V \beta(\boldsymbol{r}) \frac{\partial H(t,\boldsymbol{r})}{\partial t} dV, \tag{5}$$

where $p(t,\boldsymbol{r})$ represents the sound pressure at position $\boldsymbol{r}$ and time t; Γ is the photoacoustic efficiency factor, which is typically related to the medium's thermal expansion coefficient and specific heat capacity; $\beta(\boldsymbol{r})$ is the optical absorption coefficient of the medium at position $\boldsymbol{r}$; and $H(t,\boldsymbol{r})$ is the time distribution function of light intensity, which indicates how laser energy is absorbed by the tissue.

Such pulsed light is sufficient to produce strong initial acoustic pressure waves detectable by new types of ultrasonic probes, such as the super-low-dose photoacoustic microscopy (SLD-PAM) developed by Zhang et al., which can achieve eye or brain imaging at the 1 nJ level (Yachao Zhang 17 March 2022). Thus, theoretically, using pulsed lasers to provide energy for OPM brain mapping while performing PAI.

5.2.2.2. Hardware structure assumption of OPM-MEG and PAI light source reuse. The reuse of hardware devices can include the reuse of ADCs (von Lühmann et al., 2016), light sources (Everdell et al., 2005), etc. Discussions on ADC reuse are extensive; here, we primarily explain the hardware structure concept for the reuse of light sources that allows simultaneous, collocated detection:

For simple uniaxial configurations (where the light source is used both for pumping and measuring) in the fusion of OPM-MEG and PAI, one can refer to the structure implemented by Sheng et al. for unshielded environmental magnetic field calibration (Sheng et al., 2017). A dichroic mirror or a beam splitter tailored to specific needs can be used to divide the light source between PAI and OPM-MEG, as shown in Fig. 10(a).

For configurations with dual-pulse laser sources, particularly where the light source is separate from the pumping in the fusion of OPM-MEG and PAI, one can refer to the unshielded SERF atomic magnetometer architecture proposed by Romalis and others. In this setup, taking the Rb^{78} vapor cell as an example, the detection (780.2 nm) and pump (794.7 nm) light sources are positioned perpendicularly (Seltzer and Romalis, 2004; Seltzer, 2008), reusing the pump light source, as shown in Fig. 10(b). It is noteworthy that the dual-pulse laser configuration in Fig. 10(b) is primarily designed to optimize measurement sensitivity based on spectral characteristics. The 794.7 nm (D1 line) transitions rubidium atoms to the $5P_{1/2}$ state, effectively exciting rubidium atoms, while the 780.2 nm (D2 line) transitions rubidium atoms to the $5P_{3/2}$ state, making it more sensitive to magnetic fields and thus suitable as a probe light. Additionally, the pump light at the D1 line is also applicable for PAI imaging, allowing energy transmitted through the atomic vapor cell to be reused, thereby reducing system energy consumption and enabling a multimodal system.

Although OPM-MEG and PAI hold great potential in neuroimaging and functional imaging, their integrated application still faces engineering challenges, particularly regarding temperature effects. PAI relies on laser-induced heating to generate ultrasound signals, whereas OPM-MEG requires precise temperature control, potentially leading to

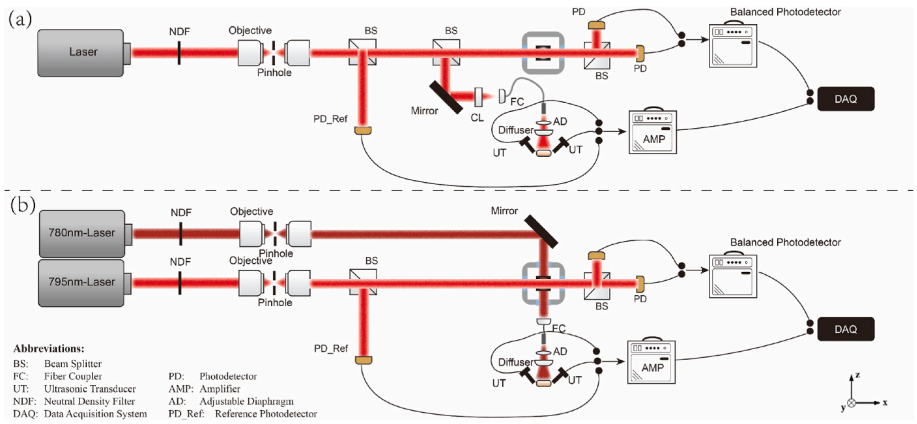

Fig. 10. Schematic of the OPM-MEG and PAI light source reuse system: (a) Schematic of a simple uniaxial configuration where the light source is used for both pumping and measurement, distributed to PAI and OPM-MEG systems via a dichroic mirror or beam splitter; (b) schematic of a dual-pulse laser source configuration, with detection and pump light sources arranged perpendicularly, reusing the pump light source in the architecture of PAI and OPM-MEG.

mutual interference. To address this issue, future research could focus on two main directions. First, exploring low-temperature SERF magnetic sensors based on a mixture of low and high atomic number elements, as vapor cells with lower atomic number elements can achieve higher ultimate sensitivity, while those with higher atomic number elements can operate at lower temperatures to maintain sufficient atomic density. A promising approach could be to use a mixture of two or more alkali metal elements pumped by a pulsed light source, as demonstrated in (Fang et al., 2014; Gerginov et al., 2017), to achieve high-precision detection near room temperature in future. Second, advancing temperature compensation algorithms. The heating model in OPM is similar to the continuous light heating structure described in (Duan et al., 2018), which can be leveraged to calibrate temperature-PA effects on PAI and improve imaging accuracy.

6. Conclusion

As neuroscience and BCI technologies rapidly evolve, wearable noninvasive BCI sensors are expanding significantly. This paper refines the definition of noninvasive BCIs and estimates the maximum comfortable weight for wearable BCI devices through basic statistical analysis.

The emergence of novel technologies such as PAI and OPM-MEG paves the way for multimodal BCI systems. Given their shared wavelength ranges and similar hardware requirements, future developments may focus on integrating key components—such as light sources and data acquisition systems, to reduce costs and enhance system flexibility.

However, thermal effects must be considered. Even with active cooling, the SERF conditions of OPM-MEG could introduce temperature fluctuations that affect PAI, which relies on localized tissue heating for mechanical expansion. Promising approaches include developing multi-element hybrid alkali metal vapor cells and using pulsed laser sources to optimize thermal stability and measurement accuracy. Addressing these challenges will be key to advancing robust multimodal noninvasive BCI systems.

CRediT authorship contribution statement

Chengpeng Chai: Writing – review & editing, Writing – original draft, Visualization, Validation, Software, Resources, Project administration, Methodology, Investigation, Formal analysis, Data curation, Conceptualization. **Xi Yang:** Writing – review & editing, Writing – original draft, Validation, Supervision, Software, Project administration, Methodology, Investigation, Formal analysis, Data curation, Conceptualization. **Yuqiao Zheng:** Writing – original draft, Visualization, Validation, Software, Resources, Project administration, Methodology, Investigation, Formal analysis, Data curation. **Md Belal Bin Heyat:** Writing – original draft, Supervision, Software, Resources, Project administration, Methodology, Funding acquisition, Formal analysis, Data curation. **Yifan Li:** Writing – original draft, Visualization, Validation, Software, Project administration, Methodology, Investigation, Formal analysis, Data curation. **Dingbo Yang:** Writing – review & editing, Visualization, Validation, Supervision, Resources, Methodology, Investigation, Funding acquisition, Data curation, Conceptualization. **Yun-Hsuan Chen:** Writing – review & editing, Writing – original draft, Visualization, Validation, Supervision, Software, Resources, Project administration, Methodology, Investigation, Funding acquisition, Formal analysis, Data curation, Conceptualization. **Mohamad Sawan:** Writing – review & editing, Writing – original draft, Visualization, Validation, Supervision, Software, Resources, Project administration, Methodology, Investigation, Funding acquisition, Formal analysis, Data curation, Conceptualization.

Informed consent statement

Not applicable.

Institutional review board statement

Not applicable.

Patent application

The authors have two patents application related to the technology discussed in this paper.

Funding

This research was funded by Westlake University [grant number 103186021801], Key Research and Development Plan of Zhejiang Province [2024C03040], STI2030-Major Projects [2022ZD0208805], "Pioneer" and "Leading Goose" R&D Program of Zhejiang [2024C03002], and the Key Project of Westlake Institute for Optoelectronics [2023GD004].

Declaration of competing interest

The authors declare the following financial interests/personal relationships which may be considered as potential competing interests: Chengpeng Chai, Xi Yang, Yun-Hsuan Chen, Mohamad Sawan has patent pending titled Multimodal Fusion Detection Device Based on Optical Pumping Technology. If there are other authors, they declare that they

have no known competing financial interests or personal relationships that could have appeared to influence the work reported in this paper.

Acknowledgements

We acknowledge the financial support provided by Westlake University, which made this research possible. We give special thanks to Dr. Jie Yang, Dr. Guoguang Rong, Dr. Sumin Bian, Dr. Nan Shao, Xurong Gao, and Yunsheng Liao for their assistance with data collection, technical support, and constructive discussions and suggestions. Thanks also to Dr. Zhong CHEN, Dr. Xue LOU, Mr. Lingyu XIAO from Instrumentation and Service Center for Molecular Sciences at Westlake University for assistance and discussion. We also thank the Elsevier Language Editing Service for their professional support in improving the clarity of this manuscript.

Data availability

Data will be made available on request.

References

Abtahi, M., Borgheai, S.B., Jafari, R., Constant, N., Diouf, R., Shahriari, Y., Mankodiya, K., 2020. IEEE Trans. Neural Syst. Rehabil. Eng. 28 (6), 1246–1253. https://doi.org/10.1109/TNSRE.2020.2987888.

Acharya, U.R., Oh, S.L., Hagiwara, Y., Tan, J.H., Adeli, H., Subha, D.P., 2018. Comput. Methods Progr. Biomed. 161, 103–113. https://doi.org/10.1016/j.cmpb.2018.04.012.

Ahlfors, S.P., Han, J., Belliveau, J.W., Hämäläinen, M.S., 2010. Brain Topogr. 23, 227–232. https://doi.org/10.1007/s10548-010-0154-x.

Ahn, S., Jun, S.C., 2017. Front. Hum. Neurosci. 11, 503. https://doi.org/10.3389/fnhum.2017.00503.

Alem, O., Benison, A.M., Barth, D.S., Kitching, J., Knappe, S., 2014. J. Neurosci. 34 (43), 14324–14327. https://doi.org/10.1523/JNEUROSCI.3495-14.2014.

Alem, O., Mhaskar, R., Jiménez-Martínez, R., Sheng, D., LeBlanc, J., Trahms, L., Sander, T., Kitching, J., Knappe, S., 2017. Opt. Express 25 (7), 7849–7858. https://doi.org/10.1364/OE.25.007849.

Allred, J., Lyman, R., Kornack, T., Romalis, M.V., 2002. Phys. Rev. Lett. 89 (13), 130801. https://doi.org/10.1103/PhysRevLett.89.130801.

Amaral, C., Mouga, S., Simões, M., Pereira, H.C., Bernardino, I., Quental, H., Playle, R., McNamara, R., Oliveira, G., Castelo-Branco, M., 2018. Front. Neurosci. 12, 477. https://doi.org/10.3389/fnins.2018.00477.

Aslam, N., Zhou, H., Urbach, E.K., Turner, M.J., Walsworth, R.L., Lukin, M.D., Park, H., 2023. Nature Rev. Phys. 5 (3), 157–169. https://doi.org/10.1038/s42254-023-00558-3.

Bai, Z., Fong, K.N., Zhang, J.J., Chan, J., Ting, K., 2020. J. NeuroEng. Rehabil. 17, 1–20. https://doi.org/10.1186/s12984-020-00686-2.

Barngrover, C., Althoff, A., DeGuzman, P., Kastner, R., 2015. IJOE 41 (1), 123–138. https://doi.org/10.1109/JOE.2015.2408471.

Barry, J.F., Turner, M.J., Schloss, J.M., Glenn, D.R., Song, Y., Lukin, M.D., Park, H., Walsworth, R.L., 2016. Proc. Natl. Acad. Sci. USA 113 (49), 14133–14138. https://doi.org/10.1073/pnas.1601513113.

Bell, W.E., Bloom, A.L., 1961. Phys. Rev. Lett. 6 (6), 280. https://doi.org/10.1103/PhysRevLett.6.280.

Bodea, S.-V., Westmeyer, G.G., 2021. Front. Neurosci. 15, 655247. https://doi.org/10.3389/fnins.2021.655247.

Bonaiuto, J.J., Rossiter, H.E., Meyer, S.S., Adams, N., Little, S., Callaghan, M.F., Dick, F., Bestmann, S., Barnes, G.R., 2018. Neuroimage 167, 372–383. https://doi.org/10.1016/j.neuroimage.2017.11.068.

Borna, A., Carter, T.R., DeRego, P., James, C.D., Schwindt, P.D., 2018. IEEE Trans. Instrum. Meas. 68 (2), 493–501. https://doi.org/10.1109/TIM.2018.2851458.

Borna, A., Carter, T.R., Goldberg, J.D., Colombo, A.P., Jau, Y.-Y., Berry, C., McKay, J., Stephen, J., Weisend, M., Schwindt, P.D., 2017. Phys. Med. Biol. 62 (23), 8909. https://doi.org/10.1088/1361-6560/aa93d1.

Boto, E., Bowtell, R., Krüger, P., Fromhold, T.M., Morris, P.G., Meyer, S.S., Barnes, G.R., Brookes, M.J., 2016. PLoS One 11 (8), e0157655. https://doi.org/10.1371/journal.pone.0157655.

Boto, E., Holmes, N., Leggett, J., Roberts, G., Shah, V., Meyer, S.S., Muñoz, L.D., Mullinger, K.J., Tierney, T.M., Bestmann, S., 2018. Nature 555 (7698), 657–661. https://doi.org/10.1038/nature26147.

Boto, E., Meyer, S.S., Shah, V., Alem, O., Knappe, S., Kruger, P., Fromhold, T.M., Lim, M., Glover, P.M., Morris, P.G., 2017. Neuroimage 149, 404–414. https://doi.org/10.1016/j.neuroimage.2017.01.034.

Boto, E., Shah, V., Hill, R.M., Rhodes, N., Osborne, J., Doyle, C., Holmes, N., Rea, M., Leggett, J., Bowtell, R., 2022. Neuroimage 252, 119027. https://doi.org/10.1016/j.neuroimage.2022.119027.

Bousseta, R., El Ouakouak, I., Gharbi, M., Regragui, F., 2018. Irbm 39 (2), 129–135. https://doi.org/10.1016/j.irbm.2018.02.001.

Brookes, M.J., Boto, E., Rea, M., Shah, V., Osborne, J., Holmes, N., Hill, R.M., Leggett, J., Rhodes, N., Bowtell, R., 2021. Neuroimage 236, 118025. https://doi.org/10.1016/j.neuroimage.2021.118025.

Brookes, M.J., Leggett, J., Rea, M., Hill, R.M., Holmes, N., Boto, E., Bowtell, R., 2022. Trends Neurosci. 45 (8), 621–634. https://doi.org/10.1016/j.tins.2022.05.008.

Burle, B., Spieser, L., Roger, C., Casini, L., Hasbroucq, T., Vidal, F., 2015. Int. J. Psychophysiol. 97 (3), 210–220. https://doi.org/10.1016/j.ijpsycho.2015.05.004.

Cao, F., An, N., Xu, W., Wang, W., Li, W., Wang, C., Xiang, M., Gao, Y., Ning, X., 2023. IEEE Trans. Med. Imag. 42 (9), 2706–2713. https://doi.org/10.1109/TMI.2023.3263167.

Casson, A.J., 2019. Biomed. Eng. Lett. 9 (1), 53–71. https://doi.org/10.1007/s13534-018-00093-6.

Cervera, M.A., Soekadar, S.R., Ushiba, J., Millán, J.d.R., Liu, M., Birbaumer, N., Garipelli, G., 2018. Ann. Clin. Translat. Neurol. 5 (5), 651–663. https://doi.org/10.1002/acn3.544.

Chae, Y., Jeong, J., Jo, S., 2012. IEEE Trans. Robot. 28 (5), 1131–1144. https://doi.org/10.1109/TRO.2012.2201310.

Chai, C., Yang, X., Gao, X., Shi, J., Wang, X., Song, H., Chen, Y.-H., Sawan, M., 2024. Front. Bioeng. Biotechnol. 12, 1452865. https://doi.org/10.3389/fbioe.2024.1452865.

Chen, K.Y., David R Bassett, J., 2005. Med. Sci. Sports Exerc. 37 (11), S490–S500. https://doi.org/10.1249/01.mss.0000185571.49104.82.

Chen, S., Liu, Q., Shu, X., Soetikno, B., Tong, S., Zhang, H.F., 2016. Biomed. Opt. Express 7 (9), 3377–3389. https://doi.org/10.1364/BOE.7.003377.

Chen, Y.-H., De Beeck, M.O., Vanderheyden, L., Carrette, E., Mihajlović, V., Vanstreels, K., Grundlehner, B., Gadeyne, S., Boon, P., Van Hoof, C., 2014. Sensors 14 (12), 23758–23780. https://doi.org/10.3390/s141223758.

Chen, Y.-H., Fang, C., Chen, E.Z., Huang, L., Sawan, M., 2021. Correlation of sleepiness scale with hemoglobin concentration variation: experimental fNIRS validation. In: 2021 Photonics & Electromagnetics Research Symposium (PIERS). IEEE, pp. 497–500. https://doi.org/10.1109/PIERS53385.2021.9694881.

Choi, J., Kim, K.T., Jeong, J.H., Kim, L., Lee, S.J., Kim, H., 2020. Sensors 20 (24), 7309. https://doi.org/10.3390/s20247309.

Cohen-Tannoudji, C., Dupont-Roc, J., Haroche, S., Laloë, F., 1970. RvPA 5 (1), 95–101. https://doi.org/10.1051/rphysap:019700050109500.

Cohen, D., 1972. Science 175 (4022), 664–666. https://doi.org/10.1126/science.175.4022.664.

Cohen, D., Cuffin, B.N., 1983. Electroencephalogr. Clin. Neurophysiol. 56 (1), 38–51. https://doi.org/10.1016/0013-4694(83)90005-6.

Cohen, D., Cuffin, B.N., Yunokuchi, K., Maniewski, R., Purcell, C., Cosgrove, G.R., Ives, J., Kennedy, J.G., Schomer, D.L., 1990. Ann. Neurol.: Off. J. Am. Neurol. Asso. Child Neurol. Soc. 28 (6), 811–817. https://doi.org/10.1002/ana.410280613.

da Silva, F.L., 2013. Neuron 80 (5), 1112–1128. https://doi.org/10.1016/j.neuron.2013.10.017.

Dang, H., Maloof, A.C., Romalis, M.V., 2010. Appl. Phys. Lett. 97 (15). https://doi.org/10.1063/1.3491215.

Del, R., Millán, J., Ferrez, P.W., Galán, F., Lew, E., Chavarriaga, R., 2008. Int. J. Pattern Recogn. Artif. Intell. 22 (5), 959–972. https://doi.org/10.1142/S0218001408006600.

Duan, T., Lan, H., Zhong, H., Zhou, M., Zhang, R., Gao, F., 2018. Opt. Lett. 43 (22), 5611–5614. https://doi.org/10.1364/OL.43.005611.

Dupont-Roc, J., Haroche, S., Cohen-Tannoudji, C., 1969. Phys. Lett. 28 (9), 638–639. https://doi.org/10.1016/0375-9601(69)90480-0.

Everdell, N., Gibson, A., Tullis, I., Vaithianathan, T., Hebden, J., Delpy, D., 2005. Rev. Sci. Instrum. 76 (9). https://doi.org/10.1063/1.2038567.

Fang, J., Li, R., Duan, L., Chen, Y., Quan, W., 2015. Rev. Sci. Instrum. 86 (7). https://doi.org/10.1063/1.4927460.

Fang, J., Wang, T., Zhang, H., Li, Y., Zou, S., 2014. Rev. Sci. Instrum. 85 (12). https://doi.org/10.1063/1.4902567.

Fang, Z., Gao, F., Jin, H., Liu, S., Wang, W., Zhang, R., Zheng, Z., Xiao, X., Tang, K., Lou, L., 2022. IEEE Trans. Biomed. Circ. Syst. 16 (6), 1075–1094. https://doi.org/10.1109/TBCAS.2022.3226290.

Fedosov, N., Shevtsov, O., Ossadtchi, A., 2021. Motor-imagery BCI with low-count of optically pumped magnetometers. In: 2021 Third International Conference Neurotechnologies and Neurointerfaces (CNN). IEEE, pp. 16–18. https://doi.org/10.1109/CNN53494.2021.9580251.

Ferrari, M., Quaresima, V., 2012. Neuroimage 63 (2), 921–935. https://doi.org/10.1016/j.neuroimage.2012.03.049.

Filosa, J.A., 2010. Front. Neuroenergetics 2, 16. https://doi.org/10.3389/fnene.2010.00016.

Fourcault, W., Romain, R., Le Gal, G., Bertrand, F., Josselin, V., Le Prado, M., Labyt, E., Palacios-Laloy, A., 2021. Opt. Express 29 (10), 14467–14475. https://doi.org/10.1364/OE.420031.

Gall, R., Mcdonald, N., Huang, X., Wears, A., Price, R.B., Ostadabbas, S., Akcakaya, M., Woody, M.L., 2024. Front. Hum. Neurosci. 18, 1360218. https://doi.org/10.3389/fnhum.2024.1360218.

Gao, X, Chen, Y H, Zeng, Z, et al., 2025. Specific endophenotypes in EEG microstates for methamphetamine use disorder[J]. Frontiers in Psychiatry 15, 1513793. https://doi.org/10.3389/fpsyt.2024.1513793.

Gerginov, V., Krzyzewski, S., Knappe, S., 2017. JOSA B 34 (7), 1429–1434. https://doi.org/10.1364/JOSAB.34.001429.

Giraldo-Suarez, E., Martínez-Vargas, J.D., Castellanos-Dominguez, G., 2016. Int. J. Neural Syst. 26 (7), 1650026. https://doi.org/10.1142/S012906571650026X.

Girouard, H., Iadecola, C., 2006. J. Appl. Physiol. 100 (1), 328–335. https://doi.org/10.1152/japplphysiol.00966.2005.

Golan, H., Makogon, B., Volkov, O., Smolyakov, Y., Hadanny, A., Efrati, S., 2020. Med. Hypotheses 136, 109510. https://doi.org/10.1016/j.mehy.2019.109510.

Griffith, W.C., Knappe, S., Kitching, J., 2010. Opt. Express 18 (26), 27167–27172. https://doi.org/10.1364/OE.18.027167.

Guggenheim, J.A., Allen, T.J., Plumb, A., Zhang, E.Z., Rodriguez-Justo, M., Punwani, S., Beard, P.C., 2015. J. Biomed. Opt. 20 (5). https://doi.org/10.1117/1.JBO.20.5.050504, 050504-050504.

Gutteling, T.P., Bonnefond, M., Clausner, T., Daligault, S., Romain, R., Mitryukovskiy, S., Fourcault, W., Josselin, V., Le Prado, M., Palacios-Laloy, A., 2023. Sensors 23 (5), 2801. https://doi.org/10.3390/s23052801.

Hämäläinen, M., Hari, R., Ilmoniemi, R.J., Knuutila, J., Lounasmaa, O.V., 1993. RvMP 65 (2), 413. https://doi.org/10.1103/RevModPhys.65.413.

Han, C.-H., Kim, Y.-W., Kim, D.Y., Kim, S.H., Nenadic, Z., Im, C.-H., 2019. J. NeuroEng. Rehabil. 16, 1–13. https://doi.org/10.1186/s12984-019-0493-0.

Hansen, P., Kringelbach, M., Salmelin, R., 2010. MEG: an Introduction to Methods. Oxford university press.

Hill, R.M., Devasagayam, J., Holmes, N., Boto, E., Shah, V., Osborne, J., Safar, K., Worcester, F., Mariani, C., Dawson, E., 2022. Neuroimage 253, 119084. https://doi.org/10.1016/j.neuroimage.2022.119084.

Hortal, E., Planelles, D., Costa, A., Iánez, E., Úbeda, A., Azorín, J.M., Fernández, E., 2015. Neurocomputing 151, 116–121. https://doi.org/10.1016/j.neucom.2014.09.078.

Horwitz, B., Friston, K.J., Taylor, J.G., 2000. Neural Netw. 13 (8–9), 829–846. https://doi.org/10.1016/S0893-6080(00)00062-9.

Hsieh, J.-C., Alawieh, H., Li, Y., Iwane, F., Zhao, L., Anderson, R., Abdullah, S.I., Tang, K. W.K., Wang, W., Pyatnitskiy, I., 2022. Biosens. Bioelectron. 218, 114756. https://doi.org/10.1016/j.bios.2022.114756.

Huang, H., Xie, Q., Pan, J., He, Y., Wen, Z., Yu, R., Li, Y., 2019. IEEE Trans. Affect. Comput. 12 (4), 832–842. https://doi.org/10.3389/fnhum.2018.00198.

Ieracitano, C., Mammone, N., Hussain, A., Morabito, F.C., 2022. Neural Comput. Appl. 34 (14), 11347–11360. https://doi.org/10.1007/s00521-020-05624-w.

Iivanainen, J., Stenroos, M., Parkkonen, L., 2017. Neuroimage 147, 542–553. https://doi.org/10.1016/j.neuroimage.2016.12.048.

Johnson, C., Schwindt, P.D., Weisend, M., 2010. Appl. Phys. Lett. 97 (24). https://doi.org/10.1063/1.3522648.

Johnson, C.N., Schwindt, P., Weisend, M., 2013. Phys. Med. Biol. 58 (17), 6065. https://doi.org/10.1088/0031-9155/58/17/6065.

Kamada, K., Sato, D., Ito, Y., Natsukawa, H., Okano, K., Mizutani, N., Kobayashi, T., 2015. Jpn. J. Appl. Phys. 54 (2), 026601. https://doi.org/10.7567/JJAP.54.026601.

Kaongoen, N., Choi, J., Jo, S., 2022. Comput. Methods Progr. Biomed. 224, 107022. https://doi.org/10.1016/j.cmpb.2022.107022.

Kasahara, K., Hoshino, H., Furusawa, Y., Sayo DaSalla, C., Honda, M., Murata, M., Hanakawa, T., 2018. Brain-Comp. Interface. 5 (2–3), 88–96. https://doi.org/10.1080/2326263X.2018.1440781.

Kassab, A., Le Lan, J., Vannasing, P., Sawan, M., 2015. Appl. Opt. 54 (3), 576–586. https://doi.org/10.1364/AO.54.000576.

Kim, K., Begus, S., Xia, H., Lee, S.-K., Jazbinsek, V., Trontelj, Z., Romalis, M.V., 2014. Neuroimage 89, 143–151. https://doi.org/10.1016/j.neuroimage.2013.10.040.

Kominis, I.K., Kornack, T.W., Allred, J.C., Romalis, M.V., 2003. Nature 422 (6932), 596–599. https://doi.org/10.1038/nature01484.

Kornack, T.W., 2005. A Test of CPT and Lorentz Symmetry Using a Potassium-Helium-3 Co-magnetometer. Princeton University.

Kozák, G., Berényi, A., 2017. Sci. Rep. 7 (1), 6300. https://doi.org/10.1038/s41598-017-06684-0.

Kumari, P., Mathew, L., Syal, P., 2017. Biosens. Bioelectron. 90, 298–307. https://doi.org/10.1016/j.bios.2016.12.001.

Labyt, E., Corsi, M.-C., Fourcault, W., Laloy, A.P., Bertrand, F., Lenouvel, F., Cauffet, G., Le Prado, M., Berger, F., Morales, S., 2018. IEEE Trans. Med. Imag. 38 (1), 90–98. https://doi.org/10.1109/TMI.2018.2856367.

Ledbetter, M., Savukov, I., Acosta, V., Budker, D., Romalis, M., 2008. Physical review A—atomic, molecular, and optical. Physics 77 (3), 033408. https://doi.org/10.1063/1.4927460.

Li, J., Zhang, Z., Wang, Z., Ren, Y., Huang, D., Wang, Q., Li, Z., 2021. Annular micro-needle array as a minimally invasive flexible dry electrode for on-Hair EEG recording. In: 2021 IEEE 34th International Conference on Micro Electro Mechanical Systems (MEMS). IEEE, pp. 270–273. https://doi.org/10.1109/MEMS51782.2021.9375246.

Li, R., Li, S., Roh, J., Wang, C., Zhang, Y., 2020a. Neurorehabilitation Neural Repair 34 (12), 1099–1110. https://doi.org/10.1177/1545968320969937.

Li, R., Potter, T., Huang, W., Zhang, Y., 2017. Front. Hum. Neurosci. 11, 462. https://doi.org/10.3389/fnhum.2017.00462.

Li, Y., Ma, Y., Ma, S., Hocke, L.M., Tong, Y., Frederick, B.d., 2020b. Neural Comput. Appl. 32 (19), 15629–15641. https://doi.org/10.1007/s00521-020-04897-5.

Li, Z., Wakai, R.T., Walker, T.G., 2006. Appl. Phys. Lett. 89 (13). https://doi.org/10.1063/1.2357553.

Limes, M., Foley, E., Kornack, T., Caliga, S., McBride, S., Braun, A., Lee, W., Lucivero, V., Romalis, M., 2020. Phys. Rev. Appl. 14 (1), 011002. https://doi.org/10.1103/PhysRevApplied.14.011002.

Lin, B.-S., Lin, B.-S., Yen, T.-H., Hsu, C.-C., Wang, Y.-C., 2019. Micromachines 10 (10), 681. https://doi.org/10.3390/mi10100681.

Lin, F.-H., Witzel, T., Ahlfors, S.P., Stufflebeam, S.M., Belliveau, J.W., Hämäläinen, M.S., 2006. Neuroimage 31 (1), 160–171. https://doi.org/10.1016/j.neuroimage.2005.11.054.

Liu, X., Wang, H., Li, Z., Qin, L., 2021a. Knowl. Base Syst. 227, 107187. https://doi.org/10.1016/j.knosys.2021.107187.

Liu, Z., Shore, J., Wang, M., Yuan, F., Buss, A., Zhao, X., 2021b. Biomed. Signal Process Control 68, 102595. https://doi.org/10.1016/j.bspc.2021.102595.

Lloyd-Fox, S., Blasi, A., Elwell, C., 2010. Neurosci. Biobehav. Rev. 34 (3), 269–284. https://doi.org/10.1016/j.neubiorev.2009.07.008.

Longo, D.L., Stefania, R., Aime, S., Oraevsky, A., 2017. Int. J. Mol. Sci. 18 (8), 1719. https://doi.org/10.3390/ijms18081719.

Lu, R.-R., Zheng, M.-X., Li, J., Gao, T.-H., Hua, X.-Y., Liu, G., Huang, S.-H., Xu, J.-G., Wu, Y., 2020. Neurosci. Lett. 718, 134727. https://doi.org/10.1016/j.neulet.2019.134727.

Mardell, L.C., Spedden, M.E., O'Neill, G.C., Tierney, T.M., Timms, R.C., Zich, C., Barnes, G.R., Bestmann, S., 2024. J. Neurosci. Methods 406, 110131. https://doi.org/10.1016/j.jneumeth.2024.110131.

Marhl, U., Wojtkiewicz, S., Sawosz, P., Jazbinšek, V., Jagličić, Z., Liebert, A., Sander, T., 2024. Combined measurement of brain activation during a motor task using fNIRS and OPM-MEG. In: European Medical and Biological Engineering Conference. Springer, pp. 170–177. https://doi.org/10.1007/978-3-031-61625-9_19.

Miao, Y., Chen, S., Zhang, X., Jin, J., Xu, R., Daly, I., Jia, J., Wang, X., Cichocki, A., Jung, T.-P., 2020. Neural Plast. 2020 (1), 8882764. https://doi.org/10.1155/2020/8882764.

Mitro, N., Argyri, K., Pavlopoulos, L., Kosyvas, D., Karagiannidis, L., Kostovasili, M., Misichroni, F., Ouzounoglou, E., Amditis, A., 2023. Sensors 23 (5), 2821. https://doi.org/10.3390/s23052821.

Møller, H., Jensen, C.B., Hammershøi, D., Sørensen, M.F., 1995. J. Audio Eng. Soc. 43 (4), 218–232.

Naseer, N., Hong, K.-S., 2015. Front. Hum. Neurosci. 9, 3. https://doi.org/10.3389/fnhum.2015.00003.

Ni, R., Vaas, M., Ren, W., Klohs, J., 2018a. Non-invasive detection of matrix-metalloproteinase activity in a mouse model of cerebral ischemia using multispectral optoacoustic tomography. Photons Plus Ultrasound: Imag. Sens. 44–49. https://doi.org/10.1117/1.NPh.5.1.015005. SPIE.

Ni, R., Vaas, M., Ren, W., Klohs, J., 2018b. Neurophotonics 5 (1). https://doi.org/10.1117/1.NPh.5.1.015005, 015005-015005.

Nicolelis, M.A., Alho, E.J., Donati, A.R., Yonamine, S., Aratanha, M.A., Bao, G., Campos, D.S., Almeida, S., Fischer, D., Shokur, S., 2022. Sci. Rep. 12 (1), 20545. https://doi.org/10.1038/s41598-022-24864-5.

Niedermeyer, E., 2011. Niedermeyer's Electroencephalography: Basic Principles, Clinical Applications, and Related Fields. Lippincott Williams & Wilkins.

Olexa, J., Kim, K.T., Saadon, J.R., Rakovec, M., Evans, M., Cohen, J., Cherian, J., Rokovec, M., 2024. Cureus 16 (7). https://doi.org/10.7759/cureus.63657.

Ometov, A., Shubina, V., Klus, L., Skibińska, J., Saafi, S., Pascacio, P., Flueratoru, L., Gaibor, D.Q., Chukhno, N., Chukhno, O., 2021. Comput. Netw. 193, 108074. https://doi.org/10.1016/j.comnet.2021.108074.

Osborne, J., Orton, J., Alem, O., Shah, V., 2018. Fully integrated standalone zero field optically pumped magnetometer for biomagnetism. Steep Dispers. Eng/ opto-atomic Prec. Metrol. XI, 89–95. https://doi.org/10.1117/12.2299197. SPIE.

Pan, J., Xie, Q., Huang, H., He, Y., Sun, Y., Yu, R., Li, Y., 2018. Front. Hum. Neurosci. 12, 198. https://doi.org/10.3389/fnhum.2018.00198.

Pang, M., Huang, Z., Wu, H., Ding, Z., Han, B., 2022a. IEEE Sens. J. 22 (5), 4514–4523. https://doi.org/10.1109/JSEN.2022.3143209.

Pang, W., Wang, Y., Guo, L., Wang, B., Lai, P., Xiao, J., 2022b. Front. Bioeng. Biotechnol. 9, 807633. https://doi.org/10.3389/fbioe.2021.807633.

Pourahmad, A., Mahnam, A., 2016. J. Med. Sign. Sens. 6 (4), 197–202.

Presacco, A., Forrester, L., Contreras-Vidal, J.L., 2011. Towards a non-invasive brain-machine interface system to restore gait function in humans. In: 2011 Annual International Conference of the IEEE Engineering in Medicine and Biology Society. IEEE, pp. 4588–4591. https://doi.org/10.1109/IEMBS.2011.6091136.

Purcell, E.M., Field, G.B., 1956. Astrophys. J. 124, 542 124, 542.

Rao, R.P., 2013. Brain-computer Interfacing: an Introduction. Cambridge University Press.

Roy, C.S., Sherrington, C.S., 1890. J. Physiol. 11 (1–2), 85. https://doi.org/10.1113/jphysiol.1890.sp000321.

Ru, X., He, K., Lyu, B., Li, D., Xu, W., Gu, W., Ma, X., Liu, J., Li, C., Li, T., 2022. Neuroimage 259, 119420. https://doi.org/10.1016/j.neuroimage.2022.119420.

Runnova, A., Selskii, A., Kiselev, A., Shamionov, R., Parsamyan, R., Zhuravlev, M., 2021. J. Personalized Med. 11 (7), 601. https://doi.org/10.3390/jpm11070601.

Russo, P., Larobina, M., Di Lillo, F., Del Vecchio, S., Mettivier, G., 2016. Nucl. Instrum. Methods Phys. Res. Sect. A Accel. Spectrom. Detect. Assoc. Equip. 809, 58–66. https://doi.org/10.1016/j.nima.2015.10.071.

Salahuddin, U., Gao, P.-X., 2021. Front. Neurosci. 15, 728178. https://doi.org/10.3389/fnins.2021.728178.

Sangani, S., Lamontagne, A., Fung, J., 2015. Prog. Brain Res. 218, 313–330. https://doi.org/10.1016/bs.pbr.2014.12.003.

Saragih, A.S., Basyiri, H.N., Raihan, M.Y., 2022. Analysis of motor imagery data from EEG device to move prosthetic hands by using deep learning classification. In: AIP Conference Proceedings. AIP Publishing. https://doi.org/10.1063/5.0098178.

Sarvas, J., 1987. Phys. Med. Biol. 32 (1), 11. https://doi.org/10.1088/0031-9155/32/1/004.

Savukov, I., Kim, Y., Shah, V., Boshier, M., 2017. Meas. Sci. Technol. 28 (3), 035104. https://doi.org/10.1088/1361-6501/aa58b4.

Savukov, I., Romalis, M.V., 2005. Phys. Rev. Lett. 94 (12), 123001. https://doi.org/10.1103/PhysRevLett.94.123001.

Schwindt, P.D., Knappe, S., Shah, V., Hollberg, L., Kitching, J., Liew, L.-A., Moreland, J., 2004. Appl. Phys. Lett. 85 (26), 6409–6411. https://doi.org/10.1063/1.1839274.

Sebastián-Romagosa, M., Cho, W., Ortner, R., Murovec, N., Von Oertzen, T., Kamada, K., Allison, B.Z., Guger, C., 2020. Front. Neurosci. 14, 591435. https://doi.org/10.3389/fnins.2020.591435.

Seltzer, S., Romalis, M., 2004. Appl. Phys. Lett. 85 (20), 4804–4806. https://doi.org/10.1063/1.1814434.

Seltzer, S.J., 2008. Developments in Alkali-Metal Atomic Magnetometry. Princeton University.
Seneviratne, S., Hu, Y., Nguyen, T., Lan, G., Khalifa, S., Thilakarathna, K., Hassan, M., Seneviratne, A., 2017. IEEE Commun. Surv. Tutor. 19 (4), 2573–2620. https://doi.org/10.1109/COMST.2017.2731979.
Shah, V., Knappe, S., Schwindt, P.D., Kitching, J., 2007. Nat. Photonics 1 (11), 649–652. https://doi.org/10.1038/nphoton.2007.201.
Shah, V.K., Wakai, R.T., 2013. Phys. Med. Biol. 58 (22), 8153. https://doi.org/10.1088/0031-9155/58/22/8153.
Shen, G., Gao, K., Zhao, N., Yi, Z., Jiang, C., Yang, B., Liu, J., 2021. JNEng 18 (6), 066047. https://doi.org/10.1088/1741-2552/ac41ab.
Sheng, D., Perry, A.R., Krzyzewski, S.P., Geller, S., Kitching, J., Knappe, S., 2017. Appl. Phys. Lett. 110 (3). https://doi.org/10.1063/1.4974349.
Shrestha, B., DeLuna, F., Anastasio, M.A., Yong Ye, J., Brey, E.M., 2020. Tissue Eng., Part B 26 (1), 79–102. https://doi.org/10.1089/ten.TEB.2019.0296.
Simmonds, M., Fertig, W., Giffard, R., 1979. ITM 15 (1), 478–481. https://doi.org/10.1109/TMAG.1979.1060155.
Sirpal, P., Kassab, A., Pouliot, P., Nguyen, D.K., Lesage, F., 2019. J. Biomed. Opt. 24 (5). https://doi.org/10.1117/1.JBO.24.5.051408, 051408-051408.
Smith, M.-C., Stinear, C.M., 2016. J. Clin. Neurosci. 31, 10–14. https://doi.org/10.1016/j.jocn.2016.01.034.
Song, Z., Fang, T., Ma, J., Zhang, Y., Le, S., Zhan, G., Zhang, X., Wang, S., Li, H., Lin, Y., 2021. Evaluation and diagnosis of brain diseases based on non-invasive BCI. In: 2021 9th International Winter Conference on Brain-Computer Interface (BCI). IEEE, pp. 1–6. https://doi.org/10.1109/BCI51272.2021.9385291.
Sotero, R.C., Trujillo-Barreto, N.J., 2008. Neuroimage 39 (1), 290–309. https://doi.org/10.1016/j.neuroimage.2007.08.001.
Sun, Y., Xixi, W., Zhou, Y., Qin, J., Bai, D., Wang, Y., Zhou, Z., 2023. IEEE Trans. Instrum. Meas. 72, 1–10. https://doi.org/10.1109/TIM.2023.3265089.
Talukdar, U., Hazarika, S.M., Gan, J.Q., 2020. JNEng 17 (1), 016020. https://doi.org/10.1088/1741-2552/ab53f1.
Tang, H., Yang, Y., Liu, Z., Li, W., Zhang, Y., Huang, Y., Kang, T., Yu, Y., Li, N., Tian, Y., 2024. Nature 630 (8015), 84–90. https://doi.org/10.1038/s41586-024-07334-y.
Tang, J., Liu, Y., Wang, Y., Zhou, B., Han, B., Zhai, Y., Liu, G., 2022. Appl. Phys. Lett. 120 (8). https://doi.org/10.1063/5.0080764.
Tang, J., Zhai, Y., Cao, L., Zhang, Y., Li, L., Zhao, B., Zhou, B., Han, B., Liu, G., 2021. Opt. Express 29 (10), 15641–15652. https://doi.org/10.1364/OE.425851.
Teplan, M., 2002. Meas. Sci. Rev. 2 (2), 1–11.
Thielen, J., Van Den Broek, P., Farquhar, J., Desain, P., 2015. PLoS One 10 (7), e0133797. https://doi.org/10.1371/journal.pone.0133797.
Tierney, T.M., Holmes, N., Mellor, S., López, J.D., Roberts, G., Hill, R.M., Boto, E., Leggett, J., Shah, V., Brookes, M.J., 2019. Neuroimage 199, 598–608. https://doi.org/10.1016/j.neuroimage.2019.05.063.
Tierney, T.M., Levy, A., Barry, D.N., Meyer, S.S., Shigihara, Y., Everatt, M., Mellor, S., Lopez, J.D., Bestmann, S., Holmes, N., 2021. Neuroimage 225, 117443. https://doi.org/10.1016/j.neuroimage.2020.117443.
Tomita, M., Gotoh, F., Sato, T., Amano, T., Tanahashi, N., Tanaka, K., Yamamoto, M., 1978. Am. J. Physiol. Heart Circ. Physiol. 235 (1), H56–H63. https://doi.org/10.1152/ajpheart.1978.235.1.H56.
Turner, R., Jones, T., 2003. Br. Med. Bull. 65 (1), 3–20. https://doi.org/10.1093/bmb/65.1.3.
Uchitel, J., Vidal-Rosas, E.E., Cooper, R.J., Zhao, H., 2021. Sensors 21 (18), 6106. https://doi.org/10.3390/s21186106.
Udovičić, G., Topić, A., Russo, M., 2016. Wearable technologies for smart environments: a review with emphasis on BCI. In: 2016 24th International Conference on Software, Telecommunications and Computer Networks (SoftCOM). IEEE, pp. 1–9. https://doi.org/10.1109/SOFTCOM.2016.7772186.
Verbaarschot, C., Tump, D., Lutu, A., Borhanazad, M., Thielen, J., van den Broek, P., Farquhar, J., Weikamp, J., Raaphorst, J., Groothuis, J.T., 2021. Clin. Neurophysiol. 132 (10), 2404–2415. https://doi.org/10.1016/j.clinph.2021.07.012.
von Lühmann, A., Müller, K.-R., 2017. Why build an integrated EEG-NIRS? About the advantages of hybrid bio-acquisition hardware. In: 2017 39th Annual International Conference of the IEEE Engineering in Medicine and Biology Society (EMBC). IEEE, pp. 4475–4478. https://doi.org/10.1249/01.mss.0000185571.49104.82.
von Lühmann, A., Wabnitz, H., Sander, T., Müller, K.-R., 2016. IEEE (Inst. Electr. Electron. Eng.) Trans. Biomed. Eng. 64 (6), 1199–1210. https://doi.org/10.1109/TBME.2016.2594127.
Waller, J.M., Maibach, H.I., 2005. Skin Res. Technol. 11 (4), 221–235. https://doi.org/10.1111/j.0909-725X.2005.00151.x.
Wang, B., Xiao, J., Jiang, H., 2014. JNEng 11 (4), 046013. https://doi.org/10.1088/1741-2560/11/4/046013.
Wang, L.V., Wu, H.-i., 2007. Biomedical Optics: Principles and Imaging. John Wiley & Sons.
Wang, M., Li, R., Zhang, R., Li, G., Zhang, D., 2018. IEEE Access 6, 26789–26798. https://doi.org/10.1109/ACCESS.2018.2825378.
Wang, Y., Xu, D., Yang, S., Xing, D., 2016. Biomed. Opt. Express 7 (2), 279–286. https://doi.org/10.1364/BOE.7.000279.
Wang, Z., Shi, N., Zhang, Y., Zheng, N., Li, H., Jiao, Y., Cheng, J., Wang, Y., Zhang, X., Chen, Y., 2023. Nat. Commun. 14 (1), 4213. https://doi.org/10.1038/s41467-023-39814-6.
Weinstock, H., 2012. SQUID Sensors: Fundamentals, Fabrication and Applications.
Williamson, S.J., Romani, G.-L., Kaufman, L., Modena, I., 2013. Biomagnetism: an Interdisciplinary Approach. Springer Science & Business Media.
Wolpaw, J.R., Millan, J.D.R., Ramsey, N.F., 2020. Handb. Clin. Neurol. 168, 15–23. https://doi.org/10.1016/B978-0-444-63934-9.00002-0.
Wyllie, R., Kauer, M., Smetana, G., Wakai, R.T., Walker, T.G., 2012. Phys. Med. Biol. 57 (9), 2619. https://doi.org/10.1088/0031-9155/57/9/2619.
Xi, L., Jin, T., Zhou, J., Carney, P., Jiang, H., 2017. Neuroimage 161, 232–240. https://doi.org/10.1016/j.neuroimage.2017.08.037.
Xie, Q., Pan, J., Chen, Y., He, Y., Ni, X., Zhang, J., Wang, F., Li, Y., Yu, R., 2018. BMC Neurol. 18, 1–12. https://doi.org/10.1186/s12883-018-1144-y.
Yachao Zhang, J.C., Zhang, J.I.E., et al., 2022. Preprint (version 1). Available at Research Square https://doi.org/10.1002/advs.202302486.
Yanagisawa, T., Fukuma, R., Seymour, B., Tanaka, M., Hosomi, K., Yamashita, O., Kishima, H., Kamitani, Y., Saitoh, Y., 2020. Neurology 95 (4), e417–e426. https://doi.org/10.1212/WNL.0000000000009858.
Yang, X, Chai, C, Chen, Y H, et al., 2025. Skull Impact on Photoacoustic Imaging of Multi-Layered Brain Tissues with Embedded Blood Vessel Under Different Optical Source Types: Modeling and Simulation[J]. Bioengineering 12 (1), 40. https://doi.org/10.3390/bioengineering12010040.
Yang, X., Chai, C., Chen, Y.-H., Sawan, M., 2024a. Bioengineering 11 (9), 916. https://doi.org/10.3390/bioengineering11090916.
Yang, X., Chai, C., Zuo, H., Chen, Y.-H., Shi, J., Ma, C., Sawan, M., 2024b. Bioengineering 11 (3), 260. https://doi.org/10.3390/bioengineering11030260.
Yang, X., Chen, Y.-H., Sawan, M., 2021a. Photoacoustic generation in human brain with embedded blood vessel: modeling and simulation. In: 2021 Photonics & Electromagnetics Research Symposium (PIERS). IEEE, pp. 1145–1152. https://doi.org/10.1109/PIERS53385.2021.9694943.
Yang, X., Chen, Y.-H., Xia, F., Sawan, M., 2021b. Photoacoustics 23, 100287. https://doi.org/10.1016/j.pacs.2021.100287.
Zhang, J., Li, J., Huang, Z., Huang, D., Yu, H., Li, Z., 2023. Health data. Science 3. https://doi.org/10.34133/hds.0096, 0096.
Zhang, R., Xiao, W., Ding, Y., Feng, Y., Peng, X., Shen, L., Sun, C., Wu, T., Wu, Y., Yang, Y., 2020. Sci. Adv. 6 (24), eaba8792. https://doi.org/10.1126/sciadv.aba8792.
Zhang, T., Guo, H., Qi, W., Xi, L., 2024. Opt Lett. 49 (6), 1524–1527. https://doi.org/10.1364/OL.514238.
Zheng, Y., Liu, M., Jiang, L., 2022. Front. Chem. 10, 1077937. https://doi.org/10.3389/fchem.2022.1077937.
Zhou, S., Gao, X., Park, G., Yang, X., Qi, B., Lin, M., Huang, H., Bian, Y., Hu, H., Chen, X., 2024. Nature 629 (8013), 810–818. https://doi.org/10.1038/s41586-024-07381-5.
Zhou, X., Sobczak, G., McKay, C.M., Litovsky, R.Y., 2020. PLoS One 15 (12), e0244186. https://doi.org/10.1371/journal.pone.0244186.
Zhuang, J., Liu, Y., Jia, Y., Huang, Y., 2019. User discomfort evaluation research on the weight and wearing mode of head-wearable device. Advances in human factors in wearable technologies and game design: proceedings of the AHFE 2018 international conferences on human factors and wearable technologies, and human factors in game design and virtual environments, held on july 21–25, 2018. In: Loews Sapphire Falls Resort at Universal Studios, Orlando, Florida, USA 9. Springer, pp. 98–110. https://doi.org/10.1007/978-3-319-94619-1_10.
Zhuang, M., Wu, Q., Wan, F., Hu, Y., 2020. J. Neurorestoratol. 8 (1), 12–25. https://doi.org/10.26599/JNR.2020.9040001.